Icarus 261 (2015) 133–148

Contents lists available at ScienceDirect

Icarus

journal homepage: www.journals.elsevier.com/icarus

Sulfur in the early martian atmosphere revisited: Experiments with a 3-D Global Climate Model

Laura Kerber [a,*], François Forget [a], Robin Wordsworth [b]

[a] Laboratoire de Météorologie Dynamique, CNRS/UPMC/IPSL, 4 place Jussieu, BP99, 75252 Paris Cedex 05, France
[b] School of Engineering and Applied Sciences, Harvard, 29 Oxford St., Cambridge, MA 02138, United States

ARTICLE INFO

Article history:
Received 7 April 2015
Revised 14 July 2015
Accepted 7 August 2015
Available online 13 August 2015

Keywords:
Mars, climate
Volcanism
Atmospheres, evolution
Atmospheres, composition
Mars, atmosphere

ABSTRACT

Volcanic SO_2 in the martian atmosphere has been invoked as a way to create a sustained or transient greenhouse during early martian history. Many modeling studies have been performed to test the feasibility of this hypothesis, resulting in a range of conclusions, from highly feasible to highly improbable. In this study we perform a wide range of simulations using the 3-D Laboratoire de Météorologie Dynamique Generic Global Climate Model (GCM) in order to place earlier results into context and to explore the sensitivity of model outcomes to parameters such as SO_2 mixing ratio, atmospheric H_2O content, background atmospheric pressure, and aerosol size, abundance, and composition. We conclude that SO_2 is incapable of creating a sustained greenhouse on early Mars, and that even in the absence of aerosols, local and daily temperatures rise above 273 K for only for limited periods with favorable background CO_2 pressures. In the presence of even small amounts of aerosols, the surface is dramatically cooled for realistic aerosol sizes. Brief, mildly warm conditions require the co-occurrence of many improbable factors, while cooling is achieved for a wide range of model parameters. Instead of causing warming, sulfur in the martian atmosphere may have caused substantial cooling, leading to the end of clement climate conditions on early Mars.

1. Introduction

In this contribution we reconsider the efficacy of a sulfur-induced greenhouse in early martian history, simulating large portions of the open parameter space and using a 3-D GCM to capture spatial and temporal variability across the globe. The goal of this work is to construct a framework so that the nuances of the "sulfur-driven warming hypothesis" can be clearly understood, and so that past and future studies can be placed in a broader context.

This study uses improved CO_2 spectroscopy and, for the first time with SO_2, radiatively active CO_2 ice clouds. We also implement improved S_8 optical properties to better model the effect of elemental sulfur aerosols on the climate. Finally, we seek to take advantage of the 3-D GCM to link global average temperatures to local/maximum temperatures and the presence of geological features that require aqueous processes to form.

One of the major aims of this study is to provide context, so we will begin by reviewing the history of the "early Mars climate question", the constraints available to models from the geologic record, and previous studies considering transient or sustained sulfur-driven warming.

1.1. Geological constraints on the early martian atmosphere

Data returned from the surface of Mars during the 1970s revealed intriguing geological evidence for a wetter early martian climate. Dendritic valley networks were discovered by Mariner 9 on ancient Noachian terrain (Sagan et al., 1973; Sharp and Malin, 1975), indicating that liquid water had flowed across the surface in the distant past. Since this time, geological investigations into early martian history have attempted to ascertain the nature and level of activity of the early martian hydrological cycle (e.g. Baker et al., 1991; Squyres and Kasting, 1994; Andrews-Hanna et al., 2010; Ehlmann et al., 2011) while atmospheric modeling efforts have focused on how the atmosphere could be warmed to temperatures great enough to sustain such activity (see Haberle, 1998; Forget et al., 2013 for reviews).

Thus far, aqueous activity has been invoked to explain numerous spatially and temporally distinct morphological and chemical signatures, including: (1) iron and magnesium-rich clays, appearing in the oldest martian terrains (e.g., Poulet et al., 2005;

* Corresponding author at: Jet Propulsion Laboratory/Caltech University, United States.
E-mail address: kerber@lmd.jussieu.fr (L. Kerber).

http://dx.doi.org/10.1016/j.icarus.2015.08.011
0019-1035/

Bibring et al., 2006; Chevrier and Mathé, 2007; Ehlmann et al., 2011); (2) high erosion rates, taking place throughout the Noachian (Schultz, 1985; Hynek and Phillips, 2001; Craddock and Howard, 2002; Howard et al., 2005; Irwin et al., 2005; Mangold et al., 2012); (3) sedimentary layering (e.g., Moore et al., 2003; Malin and Edgett, 2003; Lewis et al., 2008); (4) valley networks, dated to the late-Noachian/early-Hesperian (Wallace and Sagan, 1979; Squyres and Kasting, 1994; Carr, 1996; Fassett and Head, 2008a), and (5) iron, magnesium, and calcium-rich sulfate deposits; dated to the late-Noachian/early-Hesperian (Gendrin et al., 2005; Bibring et al., 2006; Chevrier and Mathé, 2007; Squyres and Knoll, 2005).

What constraints do these observations place upon the nature of the ancient atmosphere?

(1) Widespread **iron and magnesium-rich clays** suggest the occurrence of a period of pH-neutral aqueous alteration (e.g., Poulet et al., 2005; Bibring et al., 2006; Chevrier et al., 2007; Ehlmann et al., 2011) during the early Noachian or before. If these clays formed at the surface, they would require a climate conducive to the sustained presence of liquid water (Carter et al., 2015); however, surface formation is not strictly required (Poulet et al., 2005). The locations, assemblages, and accompanying minerals of most of the clays so far detected favor a formation in a diagenetic, hydrothermal, or magmatic system (Ehlmann et al., 2009, 2011, 2013; Meunier et al., 2012). **Aluminum-rich clays** appear in late Noachian strata: these may indicate a late-stage surface clay-forming period during which surface waters caused the leaching of mafic lithologies (Ehlmann et al., 2009, 2011, 2013). In summary, iron and magnesium rich clays of Mars do not offer clear constraints on the state of the martian atmosphere, while Al-rich clays could suggest that a limited period of surface water weathering occurred in the late Noachian (Poulet et al., 2005; Ehlmann et al., 2011; Meunier et al., 2012).

(2) **High erosion rates** (1 m/Myr; Golombek et al., 2006) taking place during the middle and late Noachian have led to degraded crater rims and significant crater infilling (Schultz, 1985; Craddock and Maxwell, 1993; Hynek and Phillips, 2001; Craddock and Howard, 2002; Irwin et al. 2005; Howard, 2007; Mangold et al., 2012). While these rates of erosion are high compared to current martian erosion rates, they are still on the lower end of terrestrial rates (Craddock et al., 1997; Irwin et al., 2005; Golombek et al. 2006). Adjacent Noachian craters of similar size can show large differences in preservation state, meaning that the process of gradation was likely slow or intermittent over ~200 million years (Craddock and Maxwell, 1993; Irwin et al., 2005). This means that while an end-Noachian "climate optimum" could potentially explain the presence of the valley networks, some mechanism is still required to explain the high erosion rates over a significant time during early martian history (Craddock et al., 1997; Irwin et al., 2005).

(3) While it is generally agreed that **sedimentary layering** requires aqueous activity over a significant amount of time, it is not simple to estimate the precise amount of time that is needed. The reason for this is that highly active hydrological systems can deposit many thick layers in short periods of time, while intermittent hydrological systems could require more time (by an order of magnitude or more) to emplace an identical set of layers (Malin and Edgett, 2003). This ambiguity is compounded by the difficulty of definitively differentiating fluvial or lacustrine sedimentary layers from volcanic, aeolian, or impact-generated layers (e.g., Malin and Edgett, 2000; Knauth et al., 2005; McCollum and Hynek, 2005). Indeed, many martian layered deposits could have resulted from an interplay between aeolian and aqueous activity in which aeolian processes delivered sediment to a basin, and groundwater cemented it (Andrews-Hanna et al., 2010). Layers such as these could form in a wide variety of climatic conditions, requiring only variations in sediment input or ground water flow (Cadieux and Kah, 2015). Sedimentary deposits that are unequivocally fluvial, such as deltas, provide some constraints. For example, the presence of river meanders in the Holden Crater delta suggests "prolonged" fluvial activity (as opposed to catastrophic floods), but the time required to form meanders can also vary greatly (from tens to thousands of years, depending on the substrate; Moore et al., 2003).

(4) **Valley networks** impose some of strongest constraints on the early martian climate. Some chains of river valleys and craters lakes extend for thousands of kilometers, requiring pressures high enough and temperatures clement enough for sustained flow (Wallace and Sagan, 1979; Squyres and Kasting, 1994; Fassett and Head, 2008a). Like sedimentary layers, it is difficult to say how much time was necessary for the valley networks to be carved. Lower flow rates over long periods of time can yield similar large-scale morphologies to higher flow rates over shorter periods. In addition, systems that are continuously active can erode the same volume of material in less time than systems with long periods of inactivity between erosion events (Barnhart et al., 2009). There are some ways to help resolve this ambiguity. First of all, while there could have been a considerable range of flow rates, the flow rate had to have been great enough to allow transport of the substrate grain size (see Hoke et al., 2011). On a larger scale, if a crater has both an inlet and an outlet channel, it means that the flow rate was rapid enough (compared to the evaporation rate) to fill up the crater and breach the other side (Fassett and Head, 2008a; see also Howard, 2007). For these craters, the minimum volume needed to breach the crater can be estimated. Given the large minimum breach volumes of these ancient lakes, it would have taken long periods hundreds to thousands of years to fill them at high, continuous flow rates, and an order of magnitude longer to fill them with a less intense hydrological regime (Fassett and Head, 2008b). The fact that many craters do *not* have exit channels places upper limits on how much water could have come at one time. Based on landscape evolution models, it appears that massive floods of water, capable of carving valley networks in tens of years, should have left more exit breaches than are currently seen on the surface (Barnhart et al., 2009). The absence of these breaches indicates that valley networks were probably formed through numerous moderate flood events rather than several large deluges, as might be expected from impact-generated climate excursions (Barnhart et al., 2009). Some valley networks have high drainage densities and extend up to drainage divides, providing evidence that these networks were fed by precipitation (rain or snowfall) (Hynek and Phillips, 2003). Importantly, a hydrological cycle is needed that is able to recycle water from the lowlands back to the highlands (i.e., the one-time emptying of a regional aquifer would not be sufficient to create the observed features) (Goldspiel and Squyres, 1991; Squyres and Kasting, 1994; Andrews-Hanna et al., 2010; Wordsworth et al., 2013). Of all of the aqueous processes identified on Mars, the valley networks and lakes provide the clearest constraints: the atmosphere must have been thicker (greater than the saturation vapor pressure of water at the given temperature Haberle et al., 2001), the surface temperature

must have been warmer (>273 K assuming pure water, tens of degrees lower for brines Fairén et al., 2009), and system recharge (likely in the form of rain or snow) must have been possible. Assuming a continuous flood of water, (at mean-annual Earth-like levels), valley networks like Paraná Valles would have taken thousands to tens of thousands of years to form (Barnhart et al., 2009). Such floods were probably episodic, however, and the periods of inactivity between them is unknown. Once again, intermittency of fluvial activity could increase the required time by several orders of magnitude (up to 10^5–10^6 yr) (Barnhart et al., 2009). Hydrological modeling of a larger number of similar valley networks yielded similar estimates (10^5–10^8), depending strongly on parameters such as substrate grainsize and slope (Hoke et al., 2011). The period of widespread valley network formation appears to have ceased near the Noachian–Hesperian boundary, with only localized valleys forming later in martian history (Fassett and Head, 2008b).

(5) Widespread iron, calcium, and magnesium **sulfates** appear in late Noachian/Hesperian terrains (Gendrin et al., 2005; Bibring et al., 2006). Three possible scenarios have been suggested to explain the presence of these minerals: first, that they are evidence of a global acidification event, in which acidic surface waters in equilibrium with a SO_2-saturated atmosphere triggered the production of massive sulfates (Fairén et al., 2004; Bibring et al., 2006; Bullock and Moore, 2007; Halevy et al., 2007; Halevy and Schrag, 2009). Second, that the sulfates were formed from the evaporation of sulfur-rich groundwater, in which case sulfate deposits would correlate with ground water seeps and springs (Andrews-Hanna et al., 2010; Andrews-Hanna and Lewis, 2011). Third, that the sulfates were formed from the oxidation of sulfide-rich basalts under an ordinary CO_2 atmosphere, in which case the sulfates would be correlated with regions of sulfide-rich basalts (Dehouck et al., 2012). Of these, only the first would provide a strong constraint on the ancient martian atmosphere.

Out of the many observations of the processes listed above, a general picture of early martian history can be imagined. Most of the Noachian period was dominated by clay formation, starting with iron and magnesium clays and then moving to aluminum-rich clays. During this time, major erosion of craters and basins was taking place. Near the Noachian/Hesperian boundary, the valley networks were formed. Sulfate deposits seem to have formed near this time as well, but they are not spatially correlated with valley networks (Bibring et al., 2006).

Historically, two major end-member hypotheses have existed to describe the early martian climate: first, that early Mars was wet and warm, with a sustained greenhouse that made it possible for liquid water to be stable on the surface for extended periods (e.g., Pollack et al., 1987; Baker et al., 1991; Hynek and Phillips, 2001; Craddock and Howard, 2002), and second, that early Mars was generally cold, and that most of the aqueous activity took place underground in hydrothermal and groundwater systems (Squyres and Kasting, 1994; Carr and Head, 2003; Ehlmann et al., 2011; Wordsworth et al., 2013). In order to satisfy the geological evidence (mainly the presence of the valley networks and lakes), even "cold Mars" scenarios must rely upon transient periods during which the surface was warm enough to allow water (or brines) to flow considerable distances (e.g., Squyres and Kasting, 1994; Segura et al., 2008; Fairén, 2010; Ehlmann et al., 2011).

1.2. The possibility of a thick, warm, CO_2 atmosphere

Warming early Mars above the freezing temperature of water has been a long-standing challenge for atmospheric modelers (see Haberle, 1998). Under the present-day Sun, a thick CO_2 atmosphere around Mars would be sufficient to warm the planet to clement temperatures (Pollack, 1979; Pollack et al., 1987; Haberle, 1998; Forget et al., 2013); however, under a faint young Sun (75% of its present luminosity Gough, 1981), even a multi-bar CO_2 atmosphere is insufficient to raise surface temperatures above 273 K. The details are summarized in a recent study by Forget et al. (2013), where the effects of a CO_2 atmosphere from 0.1 to 7 bars are explored, including the effects of different obliquities, orbital parameters, CO_2 cloud microphysical parameters, atmospheric dust loading, and surface properties. A companion paper (Wordsworth et al., 2013) described the implementation of a fully self-consistent water cycle including surface-atmosphere interactions and water ice clouds. This study concluded that even with greenhouse warming provided by water vapor and water–ice clouds, above-freezing conditions were not met for sustained periods.

1.3. The possibility of SO_2 and H_2S as warming agents

Because of the difficulty in warming the surface to clement temperatures with CO_2 and H_2O alone, volcanic gases (especially SO_2 and H_2S) have been explored as possible ways of creating either a sustained or transient greenhouse (Postawko and Kuhn, 1986; Yung et al., 1997; Johnson et al., 2008, 2009; Tian et al., 2010; Mischna et al., 2013; Halevy and Head, 2014). SO_2 would be a good greenhouse gas in the martian atmosphere because it absorbs in the infrared at wavelengths where Mars has strong emissions (Haberle, 1998). Volcanic SO_2 is an especially appealing solution to the early martian climate paradox because the martian environment is highly enriched in sulfur. Sulfur is abundant in martian basalts (Gaillard and Scaillet, 2009) and fines (up to 100 times higher than terrestrial values) (Toulmin et al., 1977; Settle, 1979; Clark et al., 1977; Yen et al., 2005; McLennan et al., 2014). Wide-spread sulfate deposits, mentioned above, exist in Valles Marineris, Meridiani Planum, Terra Sirenum, and around the north pole (Gendrin et al., 2005; Langevin et al., 2005; see review by Gaillard et al., 2013). Modeling and experimental evidence suggests that large amounts of sulfur should partition into martian melts due to their high modeled FeO contents, and a large fraction of what is dissolved will degas upon reaching the surface (Righter et al., 2009; Gaillard and Scaillet, 2009; Gaillard et al., 2013). Thus, regardless of whether sulfur-bearing gases were responsible for transient warming during the Noachian, it is likely that they were present in the atmosphere in some abundance during periods of volcanic activity. There is also direct evidence that sulfur once played a part in the martian atmosphere: mass independent sulfur fractionation values measured in the martian meteorites were found to be consistent with atmospheric photochemical fractionation (Farquhar et al., 2007). In addition, analyses conducted by the twin Mars Exploration Rovers Spirit and Opportunity revealed that the sulfur content of martian soils and dust did not usually match the sulfur content of adjacent, unweathered rock interiors (Yen et al., 2005), suggesting that the soils did not simply represent the result of in-situ basaltic weathering. Early Mars likely had an active sulfur cycle, but how this cycle affected the surface temperature, water cycle, or geological record remains a topic of debate.

1.4. The sulfur cycle

A generic planetary sulfur cycle consists of at least four different processes: outgassing via volcanism, photolysis of sulfur-bearing gases in the atmosphere, production and condensation of aerosols, and formation of surface deposits (on the Earth, the presence of the oceans and the biosphere adds additional complexity). The flux of sulfur outgassed into the atmosphere is a complex function of the

planet's level of volcanic activity, the abundance of sulfur present in the original magma, the presence of other volatile species, the oxygen fugacity, and the degassing pressure (e.g., Johnson et al., 2008; Gaillard and Scaillet, 2009). Whether sulfur gases are emitted as SO_2 or H_2S depends on the oxidation state of the magma environment. After eruption, the volcanic gases interact with the atmosphere. SO_2 and H_2S gases can interact directly with the planet's surface, or they can undergo chemical changes in the atmosphere, leading eventually to photodissociation and/or aerosol formation (Settle, 1979; Hu et al., 2013). In highly oxidizing atmospheres, like that of the Earth, SO_2 and H_2S transform into H_2SO_4, either in the gas phase through reactions with hydroxyl radicals, oxygen molecules, and water, or by dissolving directly into water droplets and undergoing aqueous oxidation, mostly by H_2O_2 (e.g., Lamb and Verlinde, 2011). In reducing atmospheres, elemental sulfur aerosols are formed following the photolysis of H_2S gas (see Hu et al., 2013). In mildly oxidizing atmospheres such as that of present-day Mars, a combination of H_2SO_4 aerosols and elemental sulfur aerosols can form, depending on the original H_2S/SO_2 ratio and the redox state of the atmosphere (Tian et al., 2010; Hu et al., 2013). Both of these processes are described in detail in Section 4.

1.5. Previous results

To establish the efficacy of a sulfur-driven greenhouse, it is first necessary to examine the radiative effect of gaseous SO_2 and H_2S on the climate. If it is found to be sufficient to warm the planet to clement temperatures, it is then necessary to establish how long this warming might last. This requires an estimate of the atmospheric lifetime of the gases and of the radiative effect of their sulfur-bearing aerosol products. The amount of SO_2 or H_2S required to produce adequate warming must be compared against estimates of the sulfur expected from mantle degassing. Finally, all of these factors must be weighed together to determine under what circumstances net warming is possible, and how likely these circumstances are to have been present on early Mars.

A number of researchers have developed models in order to assess this first point: the radiative effect of sulfur-bearing gases on the surface temperature, and whether these gases provide an adequate amount of greenhouse warming to allow liquid water to flow across the surface (Postawko and Kuhn, 1986; Johnson et al., 2008, 2009; Tian et al., 2010; Mischna et al., 2013; Halevy and Head, 2014). These efforts have mostly concentrated on the firmest of the five lines of evidence for liquid water flowing on the surface described in the introduction: the valley networks. Periodic volcanic eruptions could provide the right cadence of forcing to match the likely intermittent activity of this kind of aqueous activity (e.g., Halevy and Head, 2014). These efforts differ in the models that they used, the atmospheric pressure scenarios tested, and the amount of SO_2 introduced. In the following paragraph, we summarize the results achieved by these earlier authors, (as reported in the text and figures of their contributions) as well as the types of models used to achieve them. We highlight the results from a "base case" of a 0.5 bar atmosphere (where it is available) to facilitate intercomparison. This information is also summarized in Table 1.

Work began using 1-D radiative/convective climate models and gradually evolved to include photochemical calculations and 3-D climate simulations. Postawko and Kuhn (1986), using a latitudinally resolved energy balance model, found a warming effect of ~10 K for 1000 ppm of SO_2 in a dry CO_2 atmosphere of 0.5 bars (23 K at 1 bar). Yung et al. (1997) calculated that 0.1 ppm of SO_2 could bring surface temperatures up to ~276 K in a 2-bar atmosphere by inhibiting CO_2 condensation, but suggested that three dimensional modeling was needed in order to properly assess the full effects of cloud formation. Johnson et al. (2008) used a 3-D global circulation model and found a warming of 15–25 K for 245 ppm of SO_2 in a dry 0.5 bar atmosphere. Mischna et al. (2013), using an updated version of the same model, found 18 K of warming for a dry CO_2 atmosphere, 20 K of warming for an atmosphere with a terrestrial-like water profile, and 28 K for a saturated atmosphere, all with 245 ppm of SO_2. Tian et al. (2010) used a 1-D model to explore a wide range of SO_2 mixing values and CO_2 partial pressures, finding a warming of around ~23 K for 100 ppm in a 0.5 bar atmosphere with a fully saturated troposphere (~31 K for a 1 bar atmosphere). Halevy and Head (2014) used a 1-D radiative-convection model without heat transport to simulate the addition of small amounts of SO_2 into a dry 1-bar atmosphere, finding a global mean average warming of ~13 K for 1 ppm of SO_2. Johnson et al. (2008) also modeled the contribution of H_2S, finding a warming of 17 K for 130 ppm in a 0.5 bar atmosphere. See Table 1 for a summary of findings. The various models produce a range of values, even in the cases of models using the same parameters. Taken together, these studies portray a marginal case for the efficacy of SO_2 warming. SO_2 is found to warm several tens of degrees at most, leaving the average annual temperature well short of 273 K, but placing the liquid water within reach of some local, daily, and seasonal maximums (Mischna et al., 2013), as well as bringing the planet further into the liquid range of potential brines (Zent and Fanale, 1986; Fairén et al., 2009).

Most of the simulations above addressed the radiative effect of sulfur gases, but did not take the radiative effect of sulfate aerosol particles into account. Tian et al. (2010) ran additional simulations including H_2SO_4 and S_8 aerosols, finding that they caused a dramatic cooling effect that more than canceled the warming caused by the SO_2 gas. For this reason, the efficacy and longevity of any SO_2 warming is debated. Photochemical modeling by Johnson et al. (2009) suggested an *e*-folding time for SO_2 in the range of hundreds of years, that is to say, it would be hundreds of years for the amount of SO_2 in the atmosphere to decrease to $1/e$ of its original value. If the warming effect following an SO_2 release event also lasted for hundreds of years, it would allow ample time for some fluvial features to be formed (as discussed in the introduction). Hundreds or thousands of volcanic events spread over several million years, each with an effect lasting hundreds of years, would be a good fit for the geological data. However, Tian et al. (2010) concluded after undertaking similar modeling that while the *e*-folding time for SO_2 might be several hundred years, actual warming would last at most several months before the aerosols would begin to cool significantly. The results of previous studies have thus established that the case for an early SO_2 greenhouse is marginal, and that its success in producing warming sufficient to allow the flow of liquid water depends heavily on the details, both as far as chosen parameters and spatial and temporal variations from the average annual global mean. Many of the important parameters affecting the outcome of the models are not well constrained for early Mars. These parameters include the background atmospheric pressure, orbital parameters for Mars at the time (eccentricity, obliquity, and longitude of perihelion), the mixing ratio of SO_2 in the atmosphere, the ratio of SO_2 to H_2S, the type of aerosol formed, and the size of the aerosol particles. Because of this large parameter space, different researchers have chosen different default starting values, which has made comparisons between models difficult.

In the next section we will describe the model employed in this work, followed by a study of the radiative effects of SO_2 and H_2S on the atmosphere. We will then describe the role of sulfate and elemental sulfur aerosols and their radiative effects on the atmosphere. Finally, we will analyze how these results provide information about the early martian climate.

Table 1
Results of previous studies.

Authors	Model type	Assumed initial SO_2	Assumed initial H_2S	Pressure tested	Change in temperature	Lifetime of SO_2	Effect of aerosols?
Settle (1979)	Photochemistry/microphysics	N/A	N/A	N/A	N/A	Several hundred days	N/A
Postawko and Kuhn (1986)	1-D radiative/convective	1000 ppm	N/A	10 mbar-1 bar	500 mbar:+10 K 1000 ppm (no H_2O), est. from Fig. 3 in that work	~11 years	N/A
Johnson et al. (2008)	3-D GCM	6.14 ppm and 245 ppm for 500 mbar & eq. for 50 mbar	N/A	50 mbar and 500 mbar	500 mbar: +22 K for 245 ppm (no H_2O)	N/A	N/A
Johnson et al. (2009)	1-D photochemistry	0.01 ppm to 1 ppm	N/A	500 mb	N/A	Hundreds of years	N/A
Tian et al. (2010)	1-D radiative/convective and 1-D photoch	0–10,000 ppm	0–10,000 ppm	500 mb to 3 bar	500 mbar: +22 K for 100 ppm SO_2 with H_2O (saturated)	Several months	Net cooling (−30 K)
Mischna et al. (2013)	3-D GCM	245 ppm	N/A	500 mb	500 mbar: +18 K for 245 ppm (no H_2O)	N/A	N/A
Halevy and Head (2014)	Parameterized photochemistry based on Johnson et al. (2009)/microphysics/1-D radiative/convective model	0–10 ppm	N/A	1 bar	1 bar: +~13 K for 1 ppm (est. from Fig. 2 in that work)	Hundreds of years	Dust and H_2SO_4 combined yield ~ −13 K for 1 ppm of SO_2 (est. from Fig. 2 in that work)
Kerber et al. (current work)	3-D GCM	0–10,000 ppm	0–10,000 ppm	50 mb to 5 bar	500 mbar: +16 K for 100 ppm (no H_2O)	N/A	From −25 K to depending on particle size and opacity

2. Methods: Description of the model

The GCM used in this study, the 3-D LMD Generic Climate Model, was developed for a wide variety of planetary applications, and includes generalized radiative transfer and cloud physics (e.g., Wordsworth et al., 2011). The model uses the LMDZ 3D dynamical core (Hourdin et al., 2006), which solves the primitive equations of meteorology on an Arakawa-C grid. The model was originally derived from the LMD's present-day Mars GCM and adapted specifically to early Mars conditions (Forget et al., 2013; Wordsworth et al., 2013).

When the Mars GCM was adapted for more general planetary use, it was necessary to account more fully for the wavelength-dependent greenhouse effect of CO_2 and other gases (Wordsworth et al., 2010, 2013). The correlated-k method was used to produce a database of coefficients for use by the radiative transfer code (Wordsworth et al., 2013), using in this particular case 80 spectral bands in the longwave and 36 in the shortwave.

Control simulations were run with a $32 \times 32 \times 15$ grid, corresponding to a resolution of 11.25° longitude by 5.625° latitude in the horizontal with 15 vertical levels from the surface to ~50 km. Other resolutions were also explored to test sensitivity: the greatest difference observed between simulations of higher resolution ($64 \times 48 \times 18$ and $72 \times 36 \times 22$) was slightly more than 3 K. The vertical coordinate of the GCM uses hybrid coordinates (terrain-following sigma coordinates near the surface and pressure levels in the upper atmosphere).

Most simulations were run with 0.5 bars of background CO_2. The actual atmospheric pressure in the Late Noachian is not known. Estimates based on assumed volcanic outgassing rates range from 0.1 bars to 1.5 bars (see discussion in Forget et al., 2013). Brain and Jakosky (1998) suggested that around 3 bars of CO_2 could have been lost from the beginning of the geologic record to the present day through a combination of impact erosion, sputtering, and sequestration; however, most of the loss due to impact erosion would have taken place before the Late Noachian. According to their calculations, only ~23% of the atmosphere would be lost by impact erosion from the Late Noachian to the present day (as compared to 50–90% from the beginning of the Noachian to the present day). Combined with the effect of sputtering and loss through sequestration in the regolith and at the poles, this model would predict only about 0.32 bars during the valley network formation period. The background pressure is an important unknown parameter for Noachian climate modeling, and surface temperatures are sensitive to changes in pressure from several millibars to half a bar or more. In addition, many model atmospheres below 0.5 bars are unstable to collapse into CO_2 ice caps at low obliquities (Forget et al., 2013; Wordsworth et al., 2015). For completeness, we simulate a wide range of pressures below. All simulations included a full CO_2 cycle including CO_2 condensation and the radiative effect of CO_2 ice clouds (Forget et al., 2013). After establishing a baseline with a pure, dry, CO_2 atmosphere, simulations were run introducing SO_2 and/or H_2S at various abundances. This was done to create a standard for comparison with previous SO_2 climate studies, and to systematically explore the effect of H_2S, which has been treated only sparingly in previous works. Additional simulations were run adding the radiative effect of H_2O gas (without water ice clouds). In these cases the relative humidity profile was prescribed to be either (1) fully saturated everywhere (relatively humidity = 1), (2) a linear, terrestrial water profile (Manabe and Wetherald, 1967), or (3) the average annual relative humidity profile from an equilibrated simulation of the full water cycle (Wordsworth et al., 2013). The relative humidity in this profile is 45% near the surface with the hygropause near 8 km. In the base cases, eccentricity is set to zero and the obliquity is that of

present-day Mars. The effect of eccentricity and longitude of perihelion is discussed below, while the effect of obliquity is explored in depth in Mischna et al. (2013).

3. Results: Gases

3.1. The greenhouse effect of SO_2 and H_2S gases

Fig. 1 shows the results of simulations run for a dry CO_2 atmosphere with various abundances of SO_2 or H_2S. Simulation results from five different mixing ratios are shown: 0 ppm, 10 ppm, 100 ppm, 1000 ppm, and 10,000 ppm. While a large range of mixing ratios were explored, not all of these ratios are likely. Indeed, just to bring the atmospheric mixing ratios to 10 ppm, volcanic outgassing rates a hundred times the terrestrial average are required (Halevy and Head, 2014). On the other hand, martian outgassing has been modeled to be 10–100 times richer in sulfur than that from terrestrial magmas, and past large-scale eruption fluxes, such as the flood basalt provinces, far exceeded the terrestrial annual average value (Gaillard and Scaillet, 2009). Still, it is important to place the range of 10 ppm to 10,000 ppm into context. To provide a human point of reference, 5 ppm of SO_2 in the 1 bar atmosphere of Earth is easily noticeable and uncomfortable for healthy human individuals, while concentrations over 150 ppm can only be tolerated for several minutes before death occurs (NIOSH, 1981). The lower atmosphere of Venus, known to be rich in SO_2, has an average mixing ratio of only ~150 ppm (Esposito et al., 1997), although the higher pressure of the Venusian atmosphere means that this mixing ratio requires significantly more SO_2 than that needed to yield 150 ppm of SO_2 at the lower pressures usually hypothesized for Mars. As seen in Fig. 1, even in the case where an "unreasonably" large amount of SO_2 (10,000 ppm) is added to the atmosphere, the global annual average surface temperature does not rise above freezing anywhere on the planet for an atmosphere of 0.5 bars. H_2S provides significantly less warming than SO_2 because its main absorption features peak far from the blackbody spectrum in the 200–300 K temperature range.

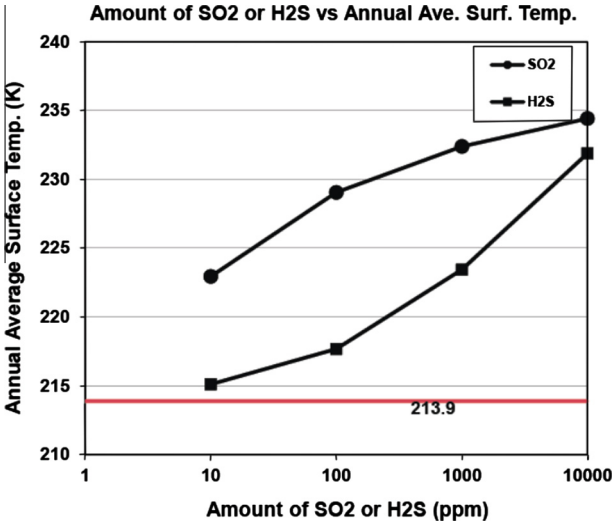

Fig. 1. The effect of varying amounts of SO_2 and H_2S gases in a dry 0.5 bar CO_2 atmosphere. The red line indicates the temperature of an atmosphere with no SO_2. H_2S is a much less powerful greenhouse gas than SO_2, except at extremely high mixing ratios. Neither gas brings surface temperatures near the melting point of water. (For interpretation of the references to color in this figure legend, the reader is referred to the web version of this article.)

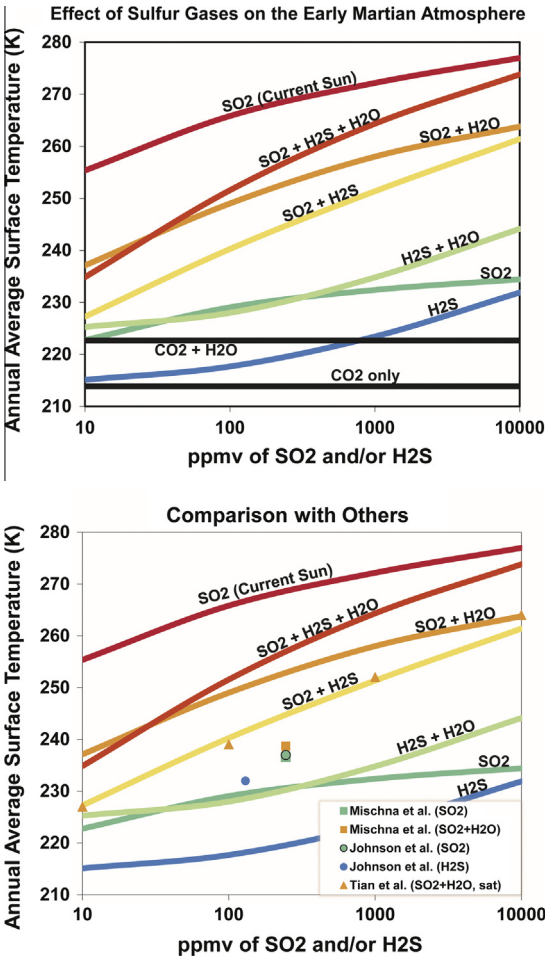

Fig. 2. (top) The effect of various volume mixing ratios of SO_2 and H_2S on the annual average surface temperature for a 0.5 bar atmosphere. All simulations were run using 75% the current solar flux, except for SO_2 (Current Sun), which shows the effect of SO_2 with 100% the current solar flux. Black lines show the baseline temperatures for simulations without SO_2 or H_2S ($CO_2 + H_2O$, and CO_2 only). (bottom) The same, but with the results of previous studies added. There is considerable variability between studies, but all simulations run under reduced solar flux conditions result in annual average temperatures below 273 K. Mixed SO_2/H_2S simulations plotted at a given ppm value were run with this ppm of each gas.

In Fig. 2a, global annual average surface temperatures are shown for a variety of gas mixtures, including SO_2, H_2S, $SO_2 + H_2O$, $H_2S + H_2O$, $SO_2 + H_2S$, and $SO_2 + H_2S + H_2O$. Fig. 2b shows the same mixtures but with the results of past studies added. In simulations where SO_2 and H_2S are present, they are mixed with a ratio of 1:1 (Gaillard and Scaillet, 2009). High temperatures in combined $SO_2 + H_2S$ simulations reflect the fact that the given ppm of *each* gas is present (i.e., the point plotted at 100 ppmv is for a simulation with 100 ppmv of H_2S and 100 ppmv of SO_2). Between studies results can vary up to 15 K (Fig. 2b); in cases the model variability is greater than the difference between simulations of different types. In no case, however, does a model produce annual average temperatures above 273 K. Fig. 2 also shows the effect of the "faint young Sun": the 25% reduction in solar intensity results in a cooling of about 35 K from the same simulations under "Current Sun" conditions. Fig. 3 shows the effects of different assumed water profiles. Five scenarios are explored: $CO_2 + H_2O$, $CO_2 + H_2O + SO_2$ (100 ppmv), $CO_2 + H_2O + SO_2$ (1000 ppmv), $CO_2 + H_2O + H_2S$ (100 ppmv), and $CO_2 + H_2O + H_2S + SO_2$ (100 ppmv for each SO_2 and H_2S). The three water profiles described in Section 2 are used: a fully saturated water profile, a humidity profile generated by

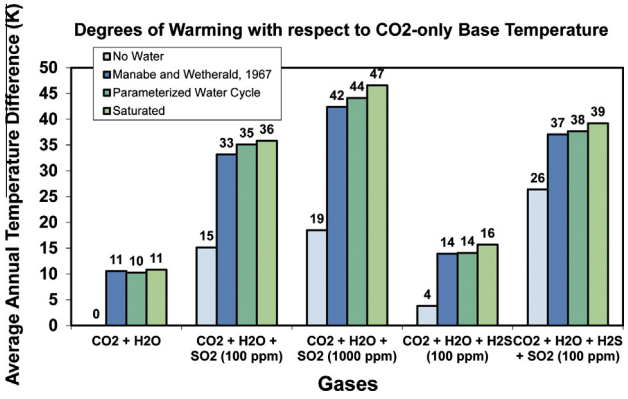

Fig. 3. The effect of SO_2 on the annual average surface temperature. Five different scenarios are shown: $CO_2 + H_2O$, $CO_2 + SO_2$, $CO_2 + H_2O + SO_2$, $CO_2 + H_2O + H_2S$, and $CO_2 + H_2O + SO_2 + H_2S$. In each case the mixing ratio of the sulfur gas is specified in parts per million (by volume). In the case of $CO_2 + H_2O + SO_2 + H_2S$, there was 100 ppm of SO_2 and 100 ppm of H_2S. Three different water schemes are compared, a saturated humidity profile (relative humidity = 1 everywhere), a humidity profile created by averaging the global relative humidity from a year-long simulation of the complete, interactive water cycle (thus reproducing the water vapor column without the effect of active clouds), and a linear profile based on terrestrial humidity data (Manabe and Wetherald, 1967). The use of different reasonable water profiles can change the final surface temperature by several degrees Kelvin. The effect of 100 ppm of SO_2 alone (+15 K) and the effect of H_2O alone (+11 K) leads to a greater total warming of 34–35 K due to the feedback effect of the temperature on the humidity profile.

taking the average relative humidity from a year-long simulation of the complete, interactive water cycle (Wordsworth et al., 2013), and a linear profile based on terrestrial humidity data (Manabe and Wetherald, 1967; Pollack et al., 1987). As shown in Fig. 3, the three water scenarios yield similar results. The combined effect of SO_2 and H_2O warming is greater than the effect of either gas alone due to the feedback of warming on the humidity profile.

As discussed above, the actual pressure during late Noachian Mars is not known. For this reason we explore the effect of SO_2 in different pressure atmospheres, ranging from 0.005 bars (close to that of today) up to 2 bars. Atmospheres with pressure higher than 3 bars are assumed to be unstable to collapse (Forget et al., 2013). Some of intermediate atmospheres could be unstable to collapse into ice caps or CO_2 glaciers, as well (for example, 50 mbars; Forget et al., 2013). The results are displayed in Fig. 4, along with results from previous studies. Each simulation was run until it reached a surface temperature equilibrium, usually five years for low pressure atmospheres and ten years for higher pressure atmospheres (>0.5 bars). From our results it can be seen that thick atmospheres (up to 2 bars) are much better than thin atmospheres for keeping the surface of Mars warm. The simulations for the top panel in Fig. 4 are for a dry atmosphere; adding the radiative effect of H_2O to the simulations drives the temperatures higher (bottom panel). For a 2-bar atmosphere with a parameterized water profile, a SO_2 mixing ratio of above 1000 ppm will bring global annual average temperatures above 273 K. Thus, if the goal is to create a warm Mars using SO_2, it could be done by carefully selecting an atmospheric pressure of 2 bars and a high SO_2 content—but whether this is what actually happened in the late Noachian is debatable. It is important to note that if an atmosphere is made twice as dense, it will take twice the amount of SO_2 to create the same mixing ratio—which might not be realistic, especially since less SO_2 is expected to degas at higher pressures than at lower pressures (Gaillard et al., 2013). In addition, the fate of such a thick late Noachian atmosphere would have to be explained: if the martian atmosphere had 2 bars of CO_2 at the end of the Noachian, where did it go? As discussed above Section 2, it may have been possible for a combination of impact erosion,

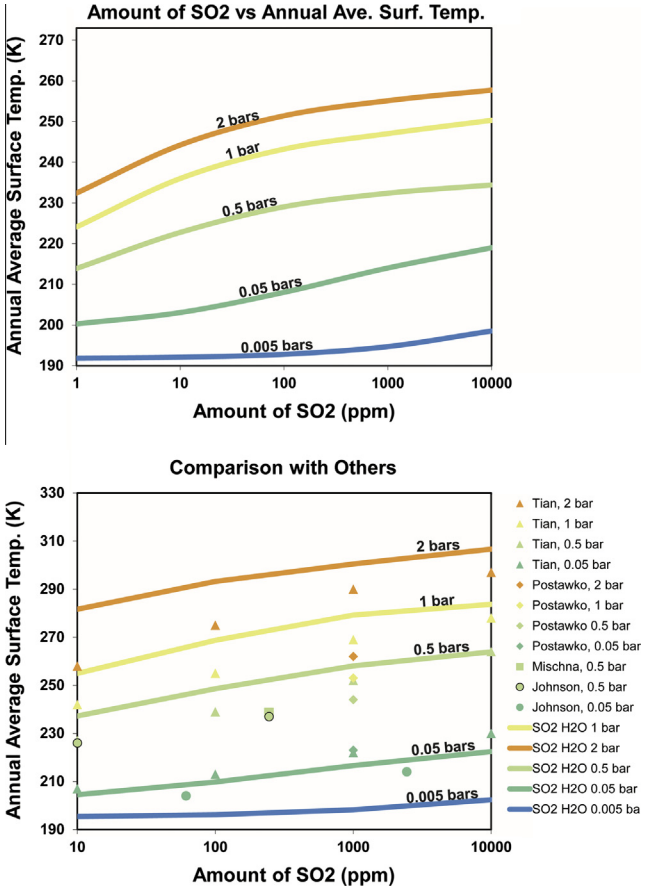

Fig. 4. (top) Annual average surface temperature according to SO_2 mixing ratio and atmospheric pressure in a dry atmosphere. (bottom) Same, but with SO_2 and H_2O and compared with relevant previous studies: Tian et al. (2010), Postawko and Kuhn (1986), Mischna et al. (2013), and Johnson et al. (2008). Our results are warmer than the others for higher temperatures. Our model slightly may overestimate temperatures at 1 and 2 bars due to a slight dependence of the temperature on dissipation at high pressures.

sputtering, and sequestration to bring the atmosphere from 3 bars at the beginning of the Noachian to 6 millibars in the present day (Brain and Jakosky, 1998), but it would be much more difficult to remove that much atmosphere beginning in the late Noachian. A better knowledge of the pressure in the atmosphere during the late Noachian is needed in order to narrow this parameter space.

To summarize, almost all background atmospheric pressures yield sub-freezing global annual average temperatures, despite the fact that aerosols have been neglected. Above-freezing global annual average temperatures are possible for a 2 bar atmosphere with H_2O and 1000 ppmv of SO_2, but this scenario is not likely. Year-round, warm, Earth-like conditions are not a likely result of SO_2 outgassing.

3.2. Spatial and temporal variations

While the global average annual surface temperature is an important metric, it is necessary to examine local and seasonal temperatures to truly characterize the possibility for liquid water on the surface. After all, the average annual temperature of Wright Valley, Antarctica ranges between 243 and 258 K, but liquid water flow takes place during the summer, allowing lakes and small rivers to form (e.g., Doran et al., 2008). In the "cold early Mars" scenario, the valley networks are hypothesized to form during

transient climate excursions, perhaps by the melting of ice accumulated during cold periods. Wordsworth et al. (2013, 2015) simulated the stability of ice on the martian surface for different orbital configurations and found that ice located in the northern lowlands would migrate to the highlands, closing the water cycle. Could SO_2 outgassing cause this ice to melt in certain places or at certain times of year? Fig. 5 shows global maps of annual average surface temperature for four scenarios: CO_2 only, $CO_2 + H_2O$, $CO_2 + SO_2$, and $CO_2 + H_2O + SO_2$. Like the pressure experiments above, simulations with H_2O were run with the average annual profile derived from the full water cycle (Wordsworth et al., 2013). The addition of water vapor greatly increases the greenhouse effect of SO_2, though average annual temperatures are still below freezing everywhere on the planet for the 100 ppm, 0.5 bar case. Average annual temperatures come within five degrees of 273 K at the bottom of Hellas basin. An addition of 1000 ppm to the 0.5 bar atmosphere would bring average annual temperatures in the lowest altitudes of Mars above freezing (Johnson et al., 2008; Righter et al., 2009), and higher pressures would also yield higher temperatures over larger parts of the surface. While a sustained greenhouse is not created for reasonable levels of SO_2 (at any pressure), warmer local and seasonal conditions are possible. Fig. 6a and b shows the fraction of the year that the surface temperature is above 273 K for the 0.5 bar case, with and without 100 ppm of SO_2, respectively. Potential for sustained flow can be better represented by the fraction of the year during which the *daily* average temperature exceeds the melting point: this is shown in Fig. 6**c**. Daily average temperatures are above freezing for fully 30% of the year at the bottom of the Hellas, though the time above 273 K remains low for most of the planet. At 2 bars, temperatures can stay above 273 K for over half the year in Hellas and some parts of the northern plains. It must be noted that these temperatures are achieved by assuming an ice-free surface albedo and thermal inertia. Additionally, they do not take into account latent heat cooling by ice sublimation and/or melting. The temperature distributions shown are appropriate assuming melting of small-scale snowpacks surrounded by bare rock surfaces, but would overestimate the melting of a large ice sheet. If the Noachian was characterized by large ice sheets, SO_2 would be less effective at melting them than we have shown. In addition, the number of condensation nuclei is a free parameter, and that used in this model (10^5 kg^{-1}) strengthens the warming provided by CO_2 ice clouds (see Forget et al., 2013, Fig. 13).

The maps here show maximum warming in areas that are different than those found by Mischna et al. (2013) for the same obliquity. This is because the areas of greatest warming are highly dependent on the assumed eccentricity of the orbit and the longitude of perihelion (i.e., if the perihelion and the summer solstice coincide for one of the planet's hemispheres, summer for this hemisphere will be slightly warmer than otherwise). Fig. 7 shows the fraction of the year above zero (like Fig. 6a and b), but for three different orbital configurations: (a) $e = 0$, (b) e = present value, longitude of perihelion at current value, (c) e = present value, longitude of perihelion opposite of the current value. The simulations by Mischna et al. (2013) can be compared to Fig. 7 (lower left; current eccentricity, current perihelion), whereas Fig. 6a and b are for

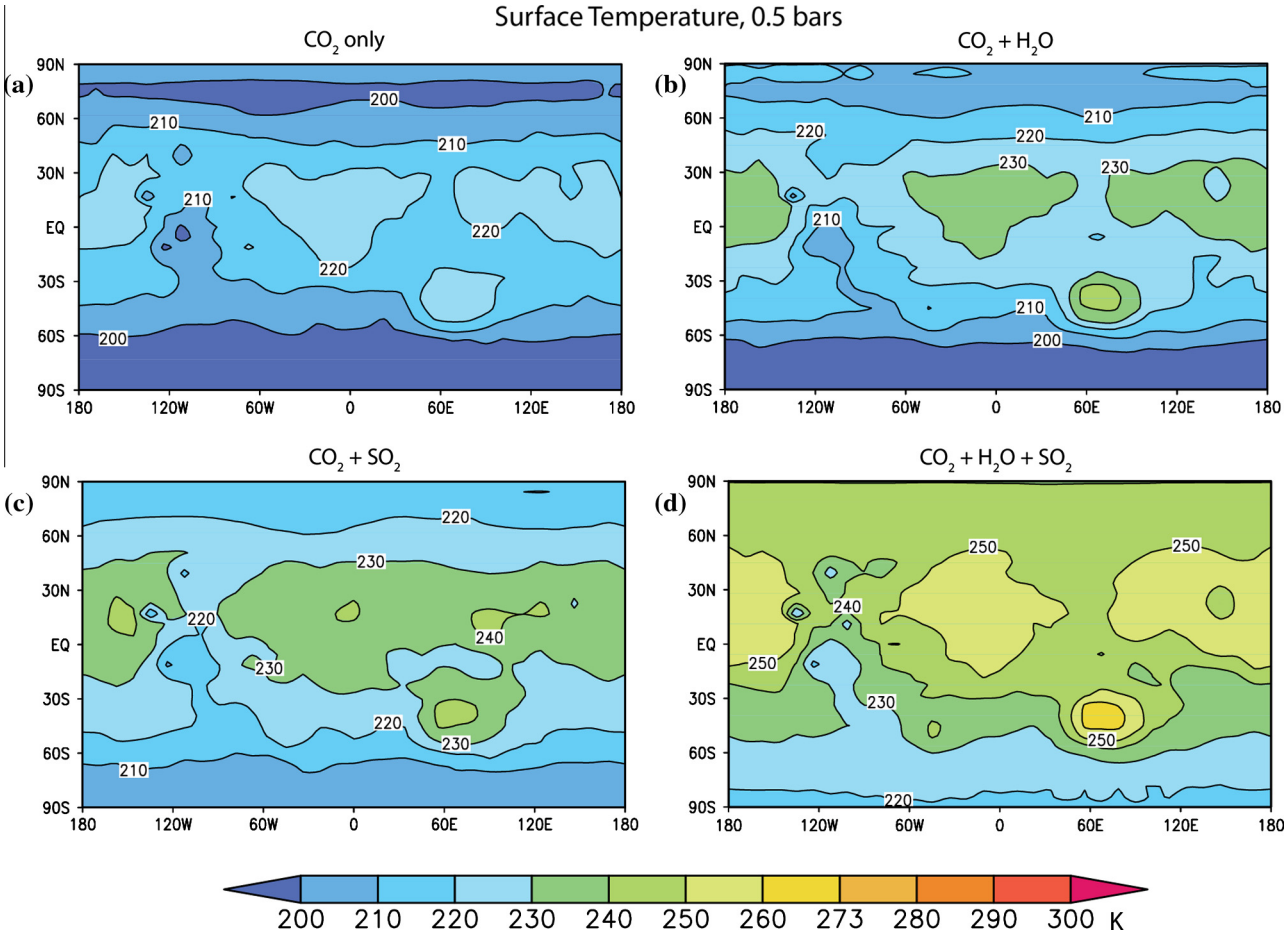

Fig. 5. Global maps showing the annual average surface temperature for (a) a control run of a CO_2-only atmosphere, (b) a run with CO_2 and H_2O, (c) a run with 100 ppm of SO_2 in a dry CO_2 atmosphere, and (d) a run with CO_2, H_2O, and 100 ppm of SO_2. An averaged relative humidity derived from the full water cycle was used for the cases with H_2O.

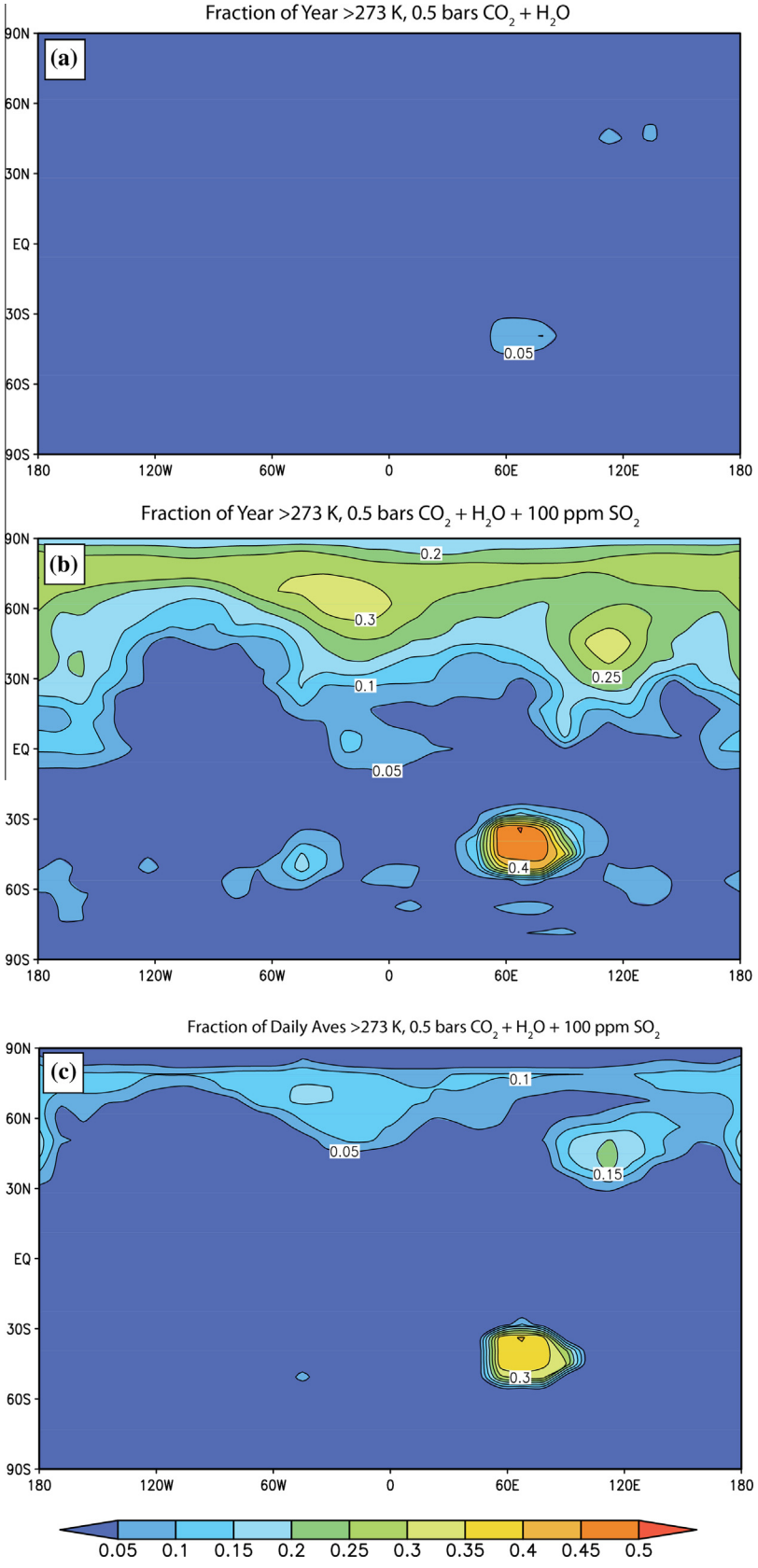

Fig. 6. (a) The fraction of year that the surface temperature rises above 273 K for a case with CO_2 and H_2O but no SO_2. (b) Like (a), but with 100 ppm of SO_2. In the bottom of Hellas basin, 45% of the year is above the melting point of water. (c) The fraction of daily averages that are above 273 K. This represents continuous clement conditions which could lead to more sustained fluvial activity. All simulations shown are for a 0.5 bar atmosphere.

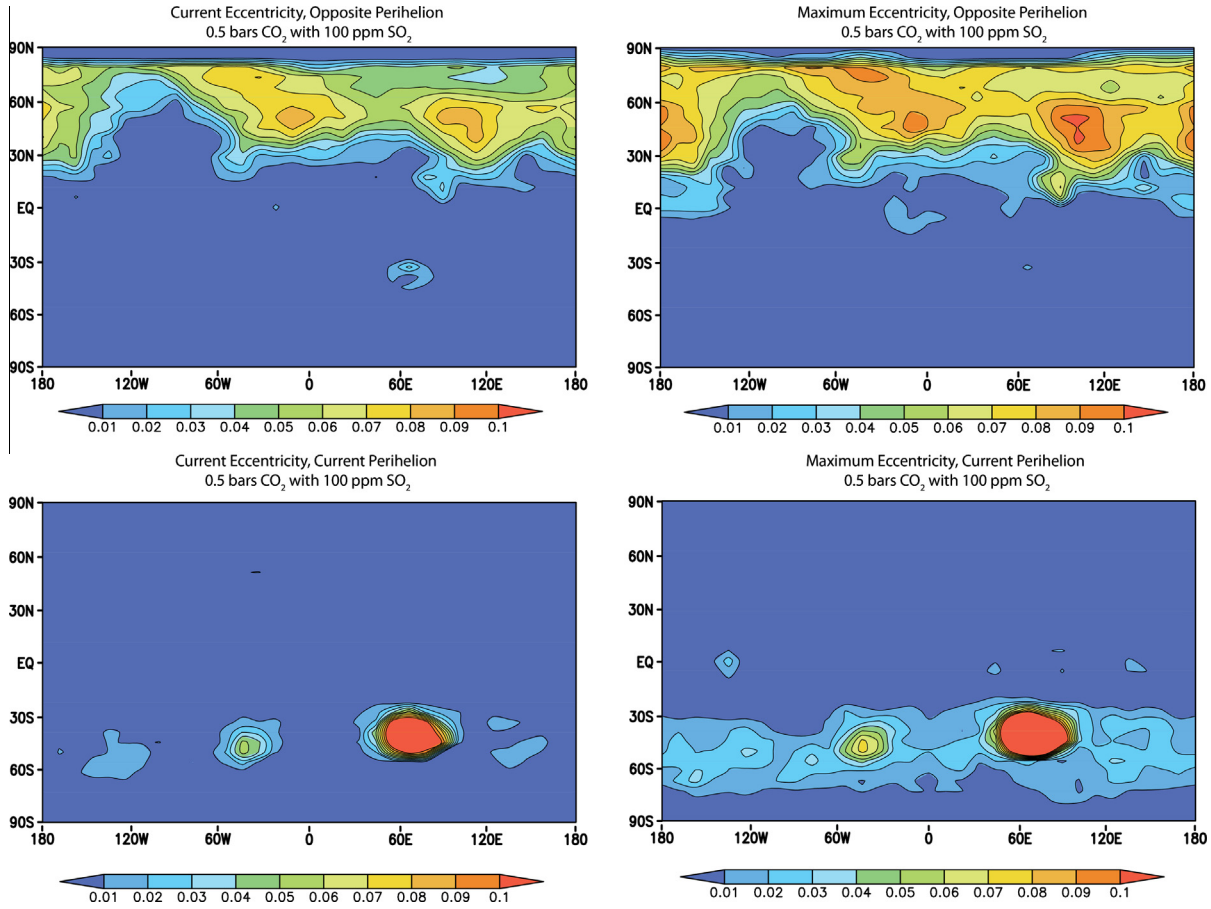

Fig. 7. The fraction of the year that the surface temperature rises above 273 K for a case with CO_2, H_2O, and SO_2 (100 ppm) for various eccentricities and longitudes of perihelion. Depending on the longitude of perihelion, different parts of the martian surface will experience above-freezing days. Increasing the eccentricity up to the maximum estimated value can expand the areas experiencing above-freezing days by a modest amount. Notice that scale is different from that of Fig. 7. Neither result is well correlated with valley network distributions (Hynek et al., 2010).

our default eccentricity of zero. Areas of greatest warming also depend heavily on obliquity, as explored in detail by Mischna et al. (2013): low obliquities concentrate warm days near the equator, while high obliquities concentrate warm days closer to the poles.

Halevy and Head (2014) find greater warming for smaller amounts of SO_2 in their 1 bar atmosphere 1-D model (~13 K for 1 ppm, versus ~9 K for 10 ppm in our results). These authors also find high annual average temperatures for subsolar latitudes, but their model does not include horizontal atmospheric heat transfer, which can decrease low-latitude temperatures by tens of degrees (Postawko and Kuhn, 1986). The 3-D model used in the current study incorporates this horizontal heat transfer, and the equatorial temperatures are accordingly lower.

In summary, we have demonstrated that SO_2 in large amounts (requiring outgassing two to three orders of magnitude higher than the terrestrial average, and forming no aerosols) can provide substantial warming. While even these large amounts of SO_2 are not enough to bring the global annual average temperature above 273 K for most atmospheres, choosing favorable background pressures allows certain geographical areas to rise above freezing for significant parts of the year. Which areas these are depend heavily upon orbital parameters such as eccentricity, longitude of perihelion, and obliquity (Mischna et al., 2013). It is possible to get >273 K temperatures in regions where valley networks are seen for low obliquities and longitudes of perihelion similar to that of the present day. Increasing the eccentricity can extend the time during which areas stay above freezing. If the Noachian atmosphere was thinner (<0.5 bars), SO_2 would not be a plausible warming agent, even in high quantities.

3.3. Brines

Brines are often mentioned only parenthetically during discussions of flowing water on the surface of Mars. However, they represent a major caveat to the above discussion (Fairén et al., 2009; Fairén, 2010). If the temperature of the planet only has to be above 245 K (Fairén, 2010) to permit brines to flow, a much larger swath of possible atmospheres and SO_2 concentrations would achieve the criteria for success. In fact, adding large amounts of H_2SO_4 to water (which would likely follow from such large concentrations of SO_2) allows it to remain liquid at temperatures significantly below the freezing point of pure water (Fig. 8) (Louie, 2005; Johnson et al., 2009; Fairén, 2010).

4. Results: Aerosols

While SO_2 can be a relatively strong greenhouse gas, as shown above, terrestrial SO_2 outgassing is usually accompanied by marked atmospheric cooling caused by the formation of sulfate aerosols. A description of the ancient martian sulfur cycle is thus not complete without taking into account the presence and effects of sulfur aerosol formation. In the following section, we explore the

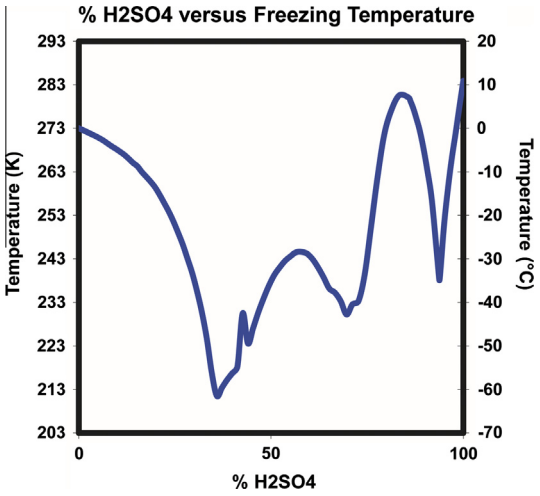

Fig. 8. Solid/liquid phase diagram for H_2SO_4–H_2O binary system. Terrestrial stratospheric aerosols are about 75% H_2SO_4 and 25% H_2O (Louie, 2005).

radiative effects of both sulfate aerosols and elemental sulfur aerosols, expanding the 1-D study done by Tian et al. (2010) to 3-D, adding improved S_8 aerosol optical properties, and including the effects of CO_2 clouds. There are three key parameters to consider regarding the radiative effects of aerosols: (1) their optical properties, (2) their size distribution (which feeds back into their optical properties), and (3) their abundance (which feeds into atmospheric opacity). If they are large enough, their vertical distribution starts to affect their greenhouse effect (like clouds), but the aerosols studied here are generally small. We begin with a short description of how H_2SO_4 and S_8 aerosols are formed and where differences between the terrestrial and martian atmospheres may introduce uncertainty.

4.1. H_2SO_4 aerosols

In the terrestrial atmosphere, H_2SO_4 is generally created in one of two different ways: through gas phase reactions, and through in-cloud aqueous chemistry. In the gas phase, H_2SO_4 is usually formed via the following reactions (e.g., Hidy, 1994; Lamb and Verlinde, 2011):

$$SO_2 + OH + M \rightarrow SO_2 \cdot OH + M \quad (1)$$

$$SO_2 \cdot OH + O_2 \rightarrow SO_3 + HO_2 \quad (2)$$

$$SO_3 + H_2O(gas) + M \rightarrow H_2SO_4 + M, \quad (3)$$

where M is any molecule (important as a collision body). Other pathways exist (e.g., Berndt et al., 2007), but they take place on Earth at comparatively slow rates and are therefore usually ignored. Previous researchers have used photochemical models to simulate this reaction in order to yield estimates for the longevity of SO_2 gas in the atmosphere, as discussed in Section 1.5 (Johnson et al., 2009; Tian et al., 2010). Gas-phase reactions create H_2SO_4 vapor, which can condense to create H_2SO_4 aerosols. The actual process by which this takes place is a subject of active research in terrestrial circles, as theoretical condensation rates are often much lower than observed rates (Finlayson-Pitts and Pitts, 2000). It is possible to form pure drops of liquid H_2SO_4, but it is energetically easier to condense H_2SO_4 gas in a binary reaction with H_2O to form concentrated sulfuric acid. On Earth, H_2SO_4 aerosols are often condensed in a ternary system with nitric acid (HNO_3) (Martin et al., 1997), allowing the formation of aerosols at vapor pressures well below that needed for homogeneous or binary nucleation (Finlayson-Pitts and Pitts, 2000). In addition, initial growth of the aerosols from nanometer clusters to detectable sizes is thought to be aided by the co-condensation of organic vapors (Finlayson-Pitts and Pitts, 2000). While the condensation and growth rate for H_2SO_4 vapor is probably fast compared to the vapor formation rate, these kinds of potentially Earth-specific processes, often hidden in Earth-derived data, can make it difficult to accurately estimate the size-distribution expected for ancient martian sulfate aerosols.

H_2SO_4 can also be formed by aqueous chemistry in liquid cloud droplets (or surface liquid water bodies), primarily through the direct dissolution of SO_2 into the water and subsequent reaction with H_2O or H_2O_2 (Claes et al., 1998):

$$H_2O_2(aq) + SO_2(aq) \rightarrow H_2SO_4(aq). \quad (4)$$

Often the H_2SO_4 created through this process is removed from the system by precipitation, but it can lead to the creation of sulfate aerosols in cases where cloud droplets evaporate before reaching the surface (Lamb and Verlinde, 2011). Whether H_2SO_4 is formed by gas chemistry or aqueous chemistry, it requires the presence of water: the greater the water content of the atmosphere, the more easily H_2SO_4 can be made. In the wet, oxidizing troposphere of the Earth, the reactions described above are fairly swift (days to weeks). In the dry stratosphere and free troposphere, it can take several months for SO_2 to be transformed into HSO_3 (Mills, 1996). H_2SO_4 aerosol particles can be delivered to the surface either through direct sedimentation ("dry" deposition) or through precipitation of cloud droplets ("wet" deposition). In the terrestrial troposphere, the oxidation of SO_2 to H_2SO_4 in cloud droplets accounts for 90% of the total chemical sink for SO_2 (Pham et al., 1995; Mills, 1996). In a cold and dry atmosphere such as that of present-day Mars, the formation of H_2SO_4 would be dominated by gas-phase chemistry, with a rate possibly limited by the availability of OH (Johnson et al., 2009) but as the amount of water in the environment increased, the role of aqueous formation of H_2SO_4 would become important. Dissolution of SO_2 into H_2O reservoirs (cloud or surface) would provide a major sink for atmospheric SO_2 (Johnson et al., 2009).

4.2. Implementation of H_2SO_4 in the model

The effect of H_2SO_4 was explored in this work by adding well-mixed, radiatively active liquid H_2SO_4 aerosols to the GCM. The amount of aerosol was scaled to create specific column opacities at particular reference wavelengths (in this case 0.55 μm to match the treatment by Tian et al. (2010)). Two sets of experiments were conducted, the first to explore the effect of H_2SO_4 particle size, and the second to explore the effect of increasing opacity. Real and imaginary indices for H_2SO_4 were taken from the HITRAN database, using the values from Hummel et al. (1988) for wavelengths between 0.2 and 0.337 μm and between 25 μm and 50 μm, while results from Palmer and Williams (1975) were used for wavelengths between 0.360 μm and 25 μm (following Tian et al. (2010) to allow for comparison).

The optical indices for H_2SO_4 have been well studied. They are dependent on temperature and acid concentration, and the equilibrium acid concentration is itself dependent on temperature, H_2O vapor pressure and the presence of basic compounds. On the Earth, sulfuric acid aerosols (mixtures of H_2O and H_2SO_4) can vary between 10 and 80 wt% H_2SO_4 in the troposphere and stratosphere (Tisdale et al., 1998). In this work, optical properties consistent with 75% H_2SO_4, 25% H_2O aerosols and a temperature of 300 K was used, as properties were available for the greatest range of wavelengths (a test was also conducted using optical properties measured at 215 K, resulting in a difference of less than 1 K). Using Mie theory, the optical indices for H_2SO_4 were used to calculate optical properties (extinction coefficient Q_{ext}, single scattering

albedo ω_0, and shape factor g) for 40 particle sizes. These properties were calculated in advance and compiled into a look-up table that was interpolated by the GCM during calculations.

4.3. S_8 aerosols

While elemental sulfur is found near volcanic fumaroles on the Earth's surface, it is rare in the Earth's atmosphere because it is rapidly oxidized. In reducing or mildly reducing environments, however, elemental sulfur, created by the photolysis of various sulfur compounds, can persist in the atmosphere (see discussion in Hu et al., 2013). Elemental sulfur aerosols are also thought to exist in the clouds of Venus (e.g., Young, 1977; Toon et al. 1982). At temperatures normally encountered in the martian atmosphere, elemental sulfur would likely exist as a crystalline solid in the form S_8. Sulfur has the tendency to form chains, meaning that elemental sulfur compounds can exist with many numbers of sulfur atoms. The S_8 form is the most stable and resistant to photochemical disruption, which is why we focus on it here (Fuller et al., 1998).

In previous work (Tian et al., 2010), optical indices for liquid S_8 were taken from Sasson et al. (1985), for wavelengths between 0.51 and 0.8 μm and derived from measurements by Bass (1953) of solid S_8 dissolved in ethyl alcohol in the UV range (0.22–0.3 μm). Indices were interpolated between 0.3 and 0.51 μm. In this work we use the optical indices for solid S_8 particles from Fuller et al. (1998). These authors collected optical indices recorded by many authors from the X-ray range out to 50 μm, thus allowing a more complete representation of the optical properties of S_8 aerosols. The difference between the two can be seen in Fig. 9. The single scattering albedo and extinction coefficients derived for various particle sizes for both S_8 and H_2SO_4 can be seen in Fig. 10. Due to the dependence of extinction cross-section on the particle radius to wavelength ratio, most of the particles are very reflective in the visible wavelengths. While small particles are generally transparent in the infrared, larger particles scatter and absorb more in the infrared.

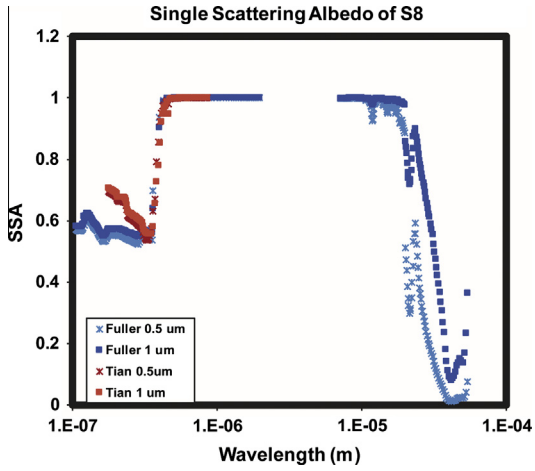

Fig. 9. Single scattering albedo for solid S_8 aerosols, using optical indices from Tian et al. (2010) and Fuller et al. (1998). Using the indices from Fuller et al. (1998) results in a lower single scattering albedo in the visible range.

4.4. The effect of aerosols

Simulations were run in dry, 0.5 bar CO_2 atmospheres (H_2O, SO_2 or H_2S) with well-mixed H_2SO_4 0.5-μm-radius particles with column opacities ranging from $\tau = 0.2$–10, producing cooling from a few degrees to ~23 K for $\tau = 10$ (Fig. 11). A single layer of H_2SO_4

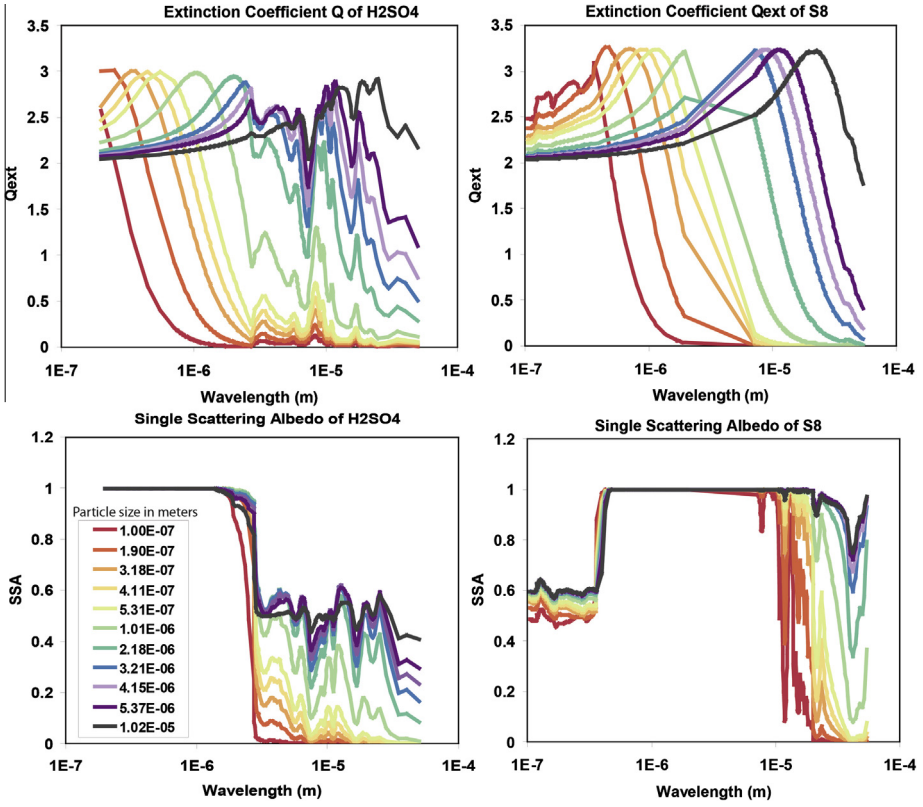

Fig. 10. Why do smaller particles cool more? Extinction coefficients (top) and single scattering albedo (bottom) for H_2SO_4 (left) and S_8 aerosols (right). Small H_2SO_4 particles are scattering in the VIS/NIR and transparent in the IR, making them ideal anti-greenhouse agents. Larger particles absorb more in the infrared, reducing their cooling effect.

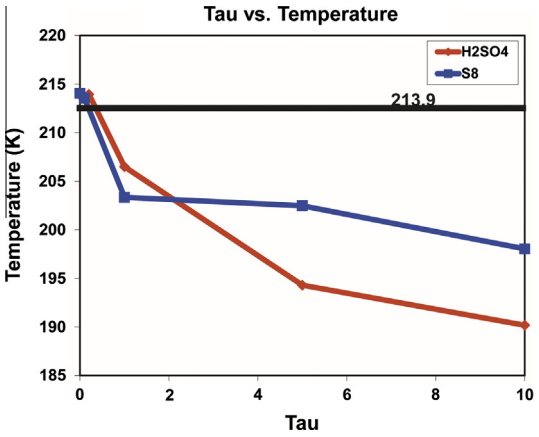

Fig. 11. The global annual average surface temperature for different optical depth values of H_2SO_4 and S_8 aerosols (particle size = 0.5 μm) for a dry 0.5 bar CO_2 atmosphere. For a given optical depth, H_2SO_4 is generally more cooling than S_8.

aerosols of the same opacity produced similar results. The cooling produced by sulfate particles was found to be somewhat less than that of Tian et al. (2010) (20 K versus 30 K) due mostly to the reduction of sulfate aerosol shortwave forcing due to the presence of CO_2 clouds (our simulations run without clouds cool 3–7 K more than simulations with clouds). Importantly, 1 ppm by mass of 1-μm-radius H_2SO_4 leads to an average global column opacity of 19, while 1 ppm by mass of 1-μm-radius S_8 leads to an average global column opacity of 11, meaning that a very small conversion of SO_2 to either aerosol can lead quickly to dramatic cooling. For example, 100 ppmv of SO_2 plus 1 ppm (by mass) of 1-μm-radius S_8 yields a global annual average temperature of 183 K, more than canceling out the original 16 K warming expected from the SO_2. Larger particles produced less cooling with some particles (radii >2 μm for H_2SO_4 and >3 μm for S_8) producing warming (Figs. 12 and 13). For 10-μm-radii S_8 aerosols, warming was up to 15 K, comparable to warming from 100 ppm of SO_2.

Are such large H_2SO_4 or S_8 aerosols reasonable? On Earth, volcanic sulfate aerosols are thought to have radii between ~0.2 and ~0.6 μm for eruptions spanning two orders of magnitude of aerosol mass, according to data simulations for numerous recent

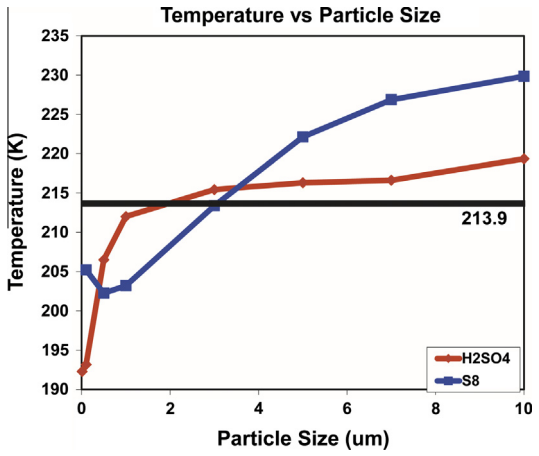

Fig. 12. The effect of a varying H_2SO_4 particle size on the average annual surface temperature for a dry 0.5 CO_2 atmosphere. Simulations were run with well-mixed particles; the column opacity in all cases was 1. Tian et al. (2010) found that S_8 particles did not cause warming at any size, but their particles were all less than 2 μm. Our results show that aerosols will cause warming if they are larger than ~2 μm for H_2SO_4 and 3 μm for S_8. Large S_8 particles cause greater warming, and S_8 aerosols are more likely to be large than H_2SO_4 aerosols.

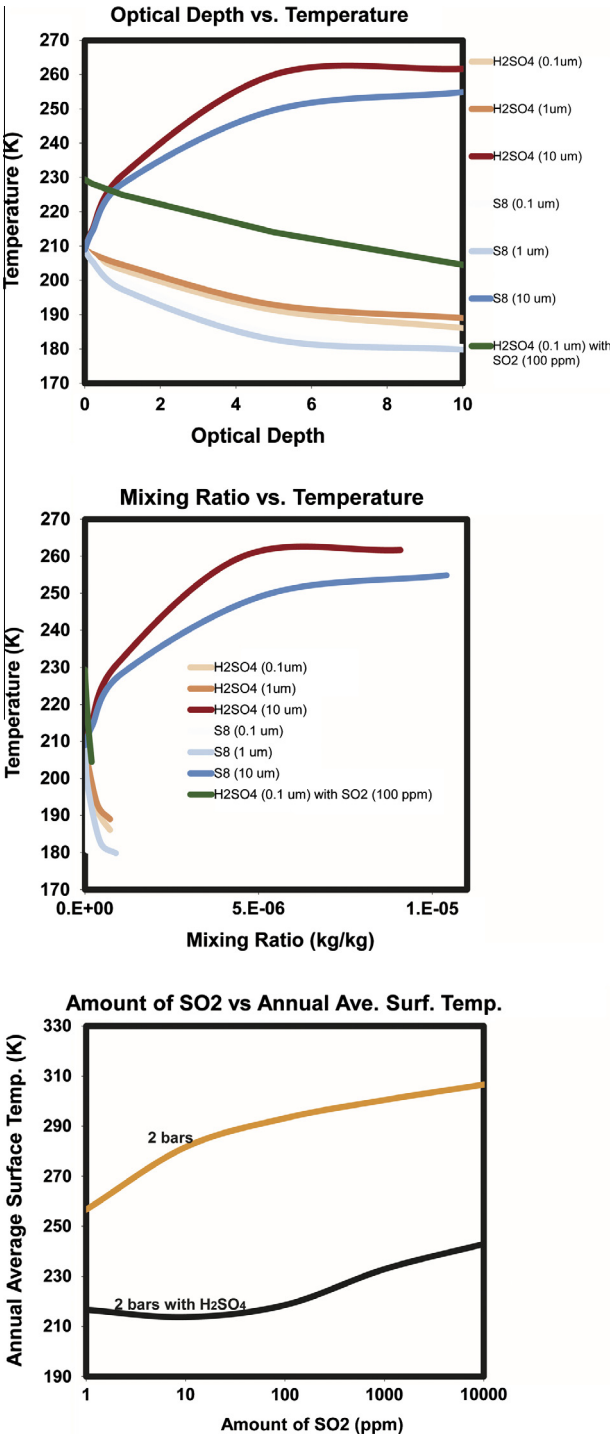

Fig. 13. The potency of H_2SO_4 and S_8 aerosols. The top panel shows the optical depths of various aerosols versus the global annual average surface temperature for a 0.5 bar dry CO_2 atmosphere. The center panel shows what mixing ratio is required to achieve an optical depth of 10 (indicated by the end of each line). Small aerosols cool up to 25 K at high optical depths (top), and they can achieve high optical depths with very small mixing ratios (center). The bottom panel shows the effect of H_2SO_4 aerosols (tau = 10) on the warmest simulation from Fig. 4.

and historic volcanic eruptions (Arfeuille et al., 2014). In terrestrial eruptions, large, dense fluxes promote the formation of aerosols up to 0.3 μm, though these are expected to sediment out of the plume before they can be dispersed world-wide (Pinto et al., 1989). Thus aerosols with radii more than 2–3 μm may not be likely. If OH radicals became depleted in the lower atmosphere, as suggested by

Johnson et al. (2009), the lifetime of SO_2 would increase (Eq. (1)), but the spread-out SO_2 would eventually form smaller, more powerfully cooling aerosols, since the average vapor pressure will be lower (Pinto et al., 1989). Observations of the upper mesosphere of Venus yielded two size distributions for H_2SO_4 aerosols: 0.1–0.3 μm (called "mode 1") and 0.4–1 μm (called "mode 2) (Sandor et al., 2010). A "mode 3" population composed of larger particles has been hypothesized, but remains controversial (e.g., Esposito et al., 1997; Sandor et al., 2010). We may conclude that even if large aerosols could form, smaller aerosols will have the strongest and most lasting effect on the climate.

S_8 aerosols could theoretically form particles that are much larger than sulfate aerosols because they form in vapor equilibrium with sulfur gas rather than in a binary system. Small drops of S_8 would have a tendency to evaporate and recondense on larger droplets because of the small droplet's high internal pressure (Young, 1977). S_8 likely exists in the current atmosphere of Venus, and large S_8 particles (10 μm) were once hypothesized to exist (Hapke and Nelson, 1975; Young, 1977), but the presence of these particles was not supported by subsequent observations (e.g., Toon et al., 1982).

The effect of aerosols, like that of SO_2, depends on the details. In most cases, aerosols would serve to drastically cool the planet. While it could have taken hundreds of years for SO_2 to decrease to $1/e$ of its original value (Johnson et al., 2009; Tian et al., 2010), we find that only a tiny amount SO_2 needs be transformed to aerosols to completely cancel out SO_2 warming (Fig. 13), in agreement with Tian et al. (2010). In special, hypothetical cases, aerosols could grow to be large (Young, 1977), in which case they could cause mild warming for a short time before sedimenting out of the atmosphere.

5. Discussion

5.1. Negative feedbacks on SO_2 warming

SO_2 is often proposed as a way to bring the surface temperature above freezing for the purpose of permitting liquid water to flow. However, water is the enemy of a sulfur greenhouse for two major reasons: (1) SO_2 is highly hydrophilic, and will be drawn down into both raindrops and surface bodies of water and (2) an abundance of water and water-related products (such as OH) speeds the transformation of SO_2 into H_2SO_4. On the other hand, the introduction of large amounts of H_2SO_4 into surface waters could allow flow to take place at temperatures well below the freezing point for pure water (Fairén et al., 2009; Johnson et al., 2009).

Gaillard et al. (2013), suggested that high (>1 bar) atmospheric pressures throughout most of the Noachian could have inhibited SO_2 outgassing in favor of H_2O and CO_2. As the atmospheric density decreased over time, the proportion of SO_2 would have increased, leading to a sulfur greenhouse and the formation of the valley networks, followed by the deposition of sulfate deposits. While this sequence matches the hypothesized chronology of the late Noachian, our results show that the same low pressures that would shift volcanic outgassing towards SO_2 release would make it increasingly difficult to achieve temperatures above freezing.

5.2. Chronology of early martian volcanism

If a sulfur-based greenhouse did exist during the late Noachian, it would have required a massive input of SO_2, as described above. Does the end of the Noachian show evidence for a peak in volcanic activity that would set it apart from the mid-Noachian or the mid-Hesperian? Evidence from crater counting suggests that several volcanic provinces (Tharsis, Syrtis Major, Apollinaris Mons, and Hadriaca Patera) were active during the end of the Noachian, but all of these centers and more (e.g. Elysium Mons, Tyrrhena Patera) were also active throughout the Hesperian, and in many cases, the Amazonian (Robbins et al., 2011). Outgassing from the construction of the Tharsis bulge has been invoked as a possible source for SO_2 (Fairén et al., 2004; Bullock and Moore, 2007; Halevy et al., 2007; Johnson et al., 2008; Gaillard and Scaillet, 2009). However, Noachian faulting patterns (Banerdt and Golombek, 2000; Golombek and Phillips, 2010) and valley network orientations (Phillips et al., 2001) may imply that the majority of the Tharsis structural load was in place by the mid-Noachian, before the valley network "climate optimum". One marked change that took place around the Noachian Hesperian boundary was the emplacement of huge volumes of Hesperian basalts, covering ~30% of the planet (Greeley and Spudis, 1981; Head et al., 2002). These volcanic plains do not generally host valley networks, however, suggesting that they post-date the end of major aqueous incision on Mars. They also post-date many lake basins—acting as post-basin fill (Fassett and Head, 2008a; Goudge et al., 2012). Better chronology regarding the activity of volcanic centers with respect to valley networks is needed in order to resolve these issues.

5.3. Unknowns and next steps

The ambiguity of the early martian SO_2 warming hypothesis is underlain by several key categories of unknowns:

(1) *The pressure in the early atmosphere.* Pressures cited in the climate modeling literature range from 0.1 bars (Postawko and Kuhn, 1986) to 4 bars (Tian et al., 2010). The results of the model are quite sensitive to pressure over such a large range. Better constraints on the pressure would be very helpful in determining whether or not SO_2 is a feasible warming agent.
(2) *The redox state of the atmosphere.* Whether the atmosphere was oxidizing or reducing determines what kinds of aerosols are expected to be produced.
(3) *The volcanic outgassing rate.* According to Gaillard et al. (2013), outgassing of S from martian basalts could range anywhere from negligible outgassing (in the case of very dry basalts), to orders of magnitude higher than terrestrial annual average rates. The outgassing rate of S plays a major role in determining how strong the SO_2 greenhouse effect is, as well as how quickly aerosols are formed and what sizes they are.
(4) *The fluvial history of Mars.* Must the SO_2 greenhouse account for both the high weathering rates of the mid-Noachian as well as the valley network formation of the late Noachian/early Hesperian? Precisely how long must the greenhouse last? Must the liquid be water, or could it have been a brine (e.g., Fairén, 2010)?

Additional modeling can help by further outlining the contours of the parameter space defined by these unknown parameters. The ideal model would be a 3-D model that combines radiative properties of gases and aerosols, photochemistry, and microphysics, in order to track the evolution of sulfur both spatially and temporally from its emission from volcanoes, to its fate in the geologic record.

6. Conclusions

Liquid water appears to be required to explain several distinct mineralogical and geomorphological features of the Noachian crust: Fe, Mg, and Al-rich clays, high erosion rates, sedimentary layering, valley networks, and sulfate deposits. Model simulations

indicate that CO_2 and H_2O alone would not be sufficient to sustain a long-term greenhouse (Forget et al., 2013; Wordsworth et al., 2013). Outgassing of large amounts of SO_2 would help to push the greenhouse closer to the melting temperature of water, potentially allowing seasonal and daily melting to take place. However, these periods of higher temperatures are only appreciable if the background pressure of the atmosphere is greater than about ~0.5 bars, and if the SO_2 mixing ratio is extremely high (>~100 ppm, less for higher pressures). Temperatures generally tend to rise with increased pressure, but increased pressure may decrease the amount of S expected to outgas from the magmas and produce a greater proportion of H_2S compared to SO_2 (Gaillard and Scaillet, 2009; Gaillard et al., 2013). Even a small amount of SO_2, transformed to aerosols, would have been sufficient to end any warming and plunge the planet into freezing conditions. In summary, while creating a transient Noachian SO_2 greenhouse is theoretically possible, it requires very specific and unlikely conditions (high pressures, high SO_2 concentrations, and large or absent aerosols). In contrast, the SO_2-driven greenhouse fails to work in a wide variety of scenarios, supporting the conclusions of Tian et al. (2010).

If volcanic SO_2 emissions did not warm the planet, what did? It is possible that other greenhouse gases such as H_2 could have warmed the planet, though this scenario also requires a large amount of background CO_2 and an extremely high H_2 mixing ratio (Ramirez et al., 2014). Potentially, high-altitude water clouds could also have played a role (Urata and Toon, 2013), although their warming effect in 3D is model-dependent (Wordsworth et al., 2013).

If volcanic SO_2 emissions did not warm the planet, what did they do? It is possible that the voluminous, sulfur-rich Hesperian flood basalts generated large quantities of sulfur aerosols, causing surface waters to become acidified and eventually evaporate or freeze. The planet would have cooled dramatically, perhaps causing any quasi-clement late Noachian conditions to come to an end.

Acknowledgments

L. Kerber would like to acknowledge CNRS and NASA PTM Grant NNX14AK33G, which both provided funding for this work.

References

Andrews-Hanna, J.C., Lewis, K.W., 2011. Early Mars hydrology: 2. Hydrological evolution in the Noachian and Hesperian epochs. J. Geophys. Res. 116, E02007. http://dx.doi.org/10.1029/2010JE003709.
Andrews-Hanna, J.C. et al., 2010. Early Mars hydrology: Meridiani playa deposits and the sedimentary record of Arabia Terra. J. Geophys. Res. 115, E06002.
Arfeuille, F. et al., 2014. Volcanic forcing for climate modeling: A new microphysics-based data set covering years 1600-present. Clim. Past 10, 359–375. http://dx.doi.org/10.5194/cp-10-359-2014.
Baker, V.R. et al., 1991. Ancient oceans, ice sheets and the hydrological cycle on Mars. Nature 352, 589–594. http://dx.doi.org/10.1038/352589a0.
Banerdt, W.B., Golombek, M.P., 2000. Tectonics of the Tharsis region of Mars: Insights from MGS topography and gravity. In: Lunar Planetary Science Conference 31, Abs. 2038.
Barnhart, C.J., Howard, A.D., Moore, J.M., 2009. Long-term precipitation and late-stage valley network formation: Landform simulations of Parana Basin, Mars. J. Geophys. Res. 114, E01003. http://dx.doi.org/10.1029/2008JE003122.
Bass, A.M., 1953. The optical absorption of sulfur. J. Chem. Phys. 21, 80–82. http://dx.doi.org/10.1063/1.1698629.
Berndt, T.O., Boge, Stratmann, F., 2007. Atmospheric H_2SO_4/H_2O Particle Formation: Mechanistic Investigations. Nucleation and Atmospheric Aerosols. Springer, Galway, Ireland.
Bibring, J.-P. et al., 2006. Global mineralogical and aqueous Mars history derived from OMEGA/Mars Express data. Science 312, 400–404.
Brain, D.A., Jakosky, B.M., 1998. Atmospheric loss since the onset of the martian geologic record: Combined role of impact erosion and sputtering. J. Geophys. Res. 103 (E10), 22689–22694.
Bullock, M.A., Moore, J.M., 2007. Atmospheric conditions on early Mars and the missing layered carbonates. Geophys. Res. Lett. 34, 19. http://dx.doi.org/10.1029/2007GL030688.
Cadieux, S.B., Kah, L.C., 2015. To what extent can intracrater layered deposits that lack clear sedimentary textures be used to infer depositional environments? Icarus 248, 526–538.
Carr, M.H., 1996. Water on Mars. Oxford University Press, p. 229.
Carr, M.H., Head, J.W., 2003. Oceans on Mars: An assessment of the observational evidence and possible fate. J. Geophys. Res. 108 (E5), 5042.
Carter, J. et al., 2015. Widespread surface weather on early Mars: A case for a warmer and wetter climate. Icarus 248, 373–382.
Chevrier, V., Mathé, P.E., 2007. Mineralogy and evolution of the surface of Mars: A review. Planet. Space Sci. 55, 289–314. http://dx.doi.org/10.1016/j.pss.2006.05.039.
Claes, M., Gysels, K., van Grieken, R., 1998. Inorganic composition of atmospheric aerosols. In: Harrison, R.M., van Grieken, R.E. (Eds.), Atmospheric Particles. Wiley, Chichester (Chapter 3).
Clark III, B.C. et al., 1977. The Viking X-ray fluorescence experiment: Analytical methods and early results. J. Geophys. Res. 82 (28), 4577–4594.
Craddock, R.A., Howard, A.D., 2002. The case for rainfall on a warm, wet early Mars. J. Geophys. Res. 107, 5111. http://dx.doi.org/10.1029/2001JE001505.
Craddock, R.A., Maxwell, T.A., 1993. Geomorphic evolution of the martian highlands through ancient fluvial processes. J. Geophys. Res. 98 (E2), 3453–3468.
Craddock, R.A., Maxwell, T.A., Howard, A.D., 1997. Crater morphometry and modification in the Sinus Sabaeus and Margaritifer Sinus regions of Mars. J. Geophys. Res. 102 (E6), 13321–13340.
Dehouck, E. et al., 2012. Evaluating the role of sulfide-weathering in the formation of sulfates or carbonates on Mars. Geochim. Cosmochim. Acta 90, 47–63.
Doran, P.T., McKay, C.P., Fountain, A.G., Nylen, T., McKnight, D.M., Jaros, C., Barrett, J. E., 2008. Hydrologic response to extreme warm and cold summers in the McMurdo Dry Valleys, East Antarctica. Antarctic Sci. 20, 499–509.
Ehlmann, B.L., Mustard, J.F., Murchie, S.L., 2009. Geologic setting of serpentine deposits on Mars. Geophys. Res. Lett. 37, L06201.
Ehlmann, B.L. et al., 2011. Nature 479, 53–60. http://dx.doi.org/10.1038/nature10582.
Ehlmann, B.L. et al., 2013. Space Sci. Rev. 174, 329–364. http://dx.doi.org/10.1007/s11213-012-9930-0.
Esposito, L.W. et al., 1997. Chemistry of lower atmosphere and clouds. In: Bougher, S.W. et al. (Eds.), Venus II: Geology, Geophysics, Atmosphere, and Solar Wind Environment. University of Arizona Press, p. 1365.
Fairén, A.G., 2010. A cold and wet Mars. Icarus 208, 165–175.
Fairén, A.G. et al., 2004. Inhibition of carbonate synthesis in acidic oceans on early Mars. Nature 431, 423–426.
Fairén, A.G. et al., 2009. Stability against freezing of aqueous solutions on early Mars. Nature 459, 401–404. http://dx.doi.org/10.1038/nature07978.
Farquhar, J., Kim, S.T., Masterson, A., 2007. Implications from sulfur isotopes of the Nakhla meteorite for the origin of sulfate on Mars. Earth Planet. Sci. Lett. 264, 1–8.
Fassett, C.I., Head, J.W., 2008a. Valley network-fed, open-basin lakes on Mars: Distribution and implications for Noachian surface and subsurface hydrology. Icarus 198, 37–56. http://dx.doi.org/10.1016/j.icarus.2008.06.016.
Fassett, C.I., Head, J.W., 2008b. The timing of martian network activity: Constraints from buffered crater counting. Icarus 195, 61–89. http://dx.doi.org/10.1016/j.icarus.2007.12.009.
Finlayson-Pitts, B.J., Pitts Jr., J.N., 2000. Chemistry of the Upper and Lower Atmosphere. Academic Press, San Diego, CA.
Forget, F. et al., 2013. 3D modeling of the early martian climate under a denser CO_2 atmosphere: Temperatures and CO_2 ice clouds. Icarus 222, 81–99.
Fuller, K.A., Downing, H.D., Querry, M.R., 1998. Orthorhombic Sulfur α-S. In: Palik, E. D. (Ed.), Handbook of Optical Constants of Solids, vol. 3. Academic Press, pp. 899–922.
Gaillard, F., Scaillet, B., 2009. The sulfur content of volcanic gases on Mars. Earth Planet. Sci. Lett. 279, 34–43.
Gaillard, F. et al., 2013. Geochemical reservoirs and timing of sulfur cycling on Mars. Space Sci. Rev. 174 (1–4), 251–300.
Gendrin, A. et al., 2005. Sulfates in martian layered terrains: The OMEGA/Mars Express view. Science 307, 1587–1591.
Goldspiel, J.M., Squyres, S.W., 1991. Ancient aqueous sedimentation of Mars. Icarus 89, 392–401. http://dx.doi.org/10.1016/0019-1035(91)90186-W.
Golombek, M.P., Phillips, R.J., 2010. Mars tectonics. In: Watters, T.R., Schultz, R.A. (Eds.), Planetary Tectonics. Cambridge University Press, Cambridge.
Golombek, M.P. et al., 2006. Erosion rates at the Mars Exploration Rover landing sites and long-term climate change on Mars. J. Geophys. Res. 111, E12S10. http://dx.doi.org/10.1029/2006JE002754.
Goudge, T.A. et al., 2012. An analysis of open-basin lake deposits on Mars: Evidence for the nature of associated lacustrine deposits and post-lacustrine modification processes. Icarus 219, 211–229.
Gough, D.O., 1981. Solar interior structure and luminosity variations. Solar Phys. 74, 21–34.
Greeley, R., Spudis, P.D., 1981. Volcanism on Mars. Rev. Geophys. 19, 13–41.
Haberle, R.M., 1998. Early Mars climate models. J. Geophys. Res. 103, 28467–28479.
Haberle, R.M., McKay, C.P., Schaeffer, J., Cabrol, N.A., Grin, E.A., Zent, A.P., Quinn, R., 2001. On the possibility of liquid water on present-day Mars. J. Geophys. Res. 106 (E10), 23317–23326.
Halevy, I., Head, J.W., 2014. Episodic warming of early Mars by punctuated volcanism. Nat. Geosci. 7. http://dx.doi.org/10.1038/NGEO2293.
Halevy, I., Schrag, D.P., 2009. Sulfur dioxide inhibits calcium carbonate precipitation: Implications for early Mars and Earth. Geophys. Res. Lett. 36, L23201. http://dx.doi.org/10.1029/2009GL040792.

Halevy, I., Zuber, M.T., Schrag, D.P., 2007. A sulfur dioxide climate feedback on early Mars. Science 318, 1903–1907.
Hapke, B., Nelson, R., 1975. Evidence for an elemental sulfur component of the clouds from Venus spectrophotometry. J. Atmos. Sci. 32, 1212–1218.
Head III, J.W., Kreslavsky, M.A., Pratt, S., 2002. Northern lowlands of Mars: Evidence for widespread volcanic flooding and tectonic deformation in the Hesperian period. J. Geophys. Res. 107 (E1). http://dx.doi.org/10.1029/2000JE001445.
Hidy, G.M., 1994. Atmospheric sulfur and nitrogen oxides: Eastern North American Source-Receptor Relationships, p. 369.
Hoke, M.R.T., Hynek, B.M., Tucker, G.E., 2011. Formation timescales of large martian valley networks. Earth Planet. Lett. 312, 1–12.
Hourdin, F. et al., 2006. The LMDZ4 general circulation model: Climate performance and sensitivity to parameterized physics with emphasis on tropical convection. Clim. Dyn. 27, 787–813.
Howard, A.D., 2007. Simulating the development of martian highland landscapes through the interaction of impact cratering, fluvial erosion, and variable hydrologic forcing. Geomorphology 91, 332–363.
Howard, A.D. et al., 2005. An intense terminal epoch of widespread fluvial activity on early Mars: 1. Valley network incision and associate deposits. J. Geophys. Res. 110, E12S14. http://dx.doi.org/10.1029/2005JE002459.
Hu, R., Seager, S., Bains, W., 2013. Photochemistry in terrestrial exoplanet atmospheres II. H_2S and SO_2 photochemistry in anoxic atmospheres. Astrophys. J. 769. http://dx.doi.org/10.1088/0004-637X/769/1/6.
Hummel, J.R., Shettle, E.P., Longtin, D.R., 1988. A New Background Stratospheric Aerosol Model for Use in Atmospheric Radiation Models, AFGL-TR-88-1066. Air Force Geophysics Laboratory, Hanscom AFB, MA, August 1988.
Hynek, B.M., Phillips, R.J., 2001. Evidence for extensive denudation of the martian highlands. Geology 29, 407–410. http://dx.doi.org/10.1130/0091-7613(2001)029.
Hynek, B.M., Phillips, R.J., 2003. New data reveal mature, integrated drainage systems on Mars indicative of past precipitation. Geology 31 (9), 757–760. http://dx.doi.org/10.1130/G19607.1.
Hynek, B.M., Hoke, M.R.T., Beach, M., 2010. Updated global map of martian valley networks and implications for climate and hydrologic processes. J. Geophys. Res. 115, E09008. http://dx.doi.org/10.1029/2009JE003548.
Irwin III, R.P. et al., 2005. An intense terminal epoch of widespread fluvial activity on early Mars: 2. Increased runoff and paleolake development. J. Geophys. Res. 110, E12S15. http://dx.doi.org/10.1029/2005JE002460.
Johnson, S.S. et al., 2008. Sulfur-induced greenhouse warming on early Mars. J. Geophys. Res. 113, E08005. http://dx.doi.org/10.1029/2007JE002962.
Johnson, S.S., Pavlov, A.A., Mischna, M.A., 2009. Fate of SO_2 in the ancient martian atmosphere: Implications for transient greenhouse warming. J. Geophys. Res. 114, E11. http://dx.doi.org/10.1029/2008JE003313.
Knauth, L.P., Burt, D.M., Wohletz, K.H., 2005. Impact origin of sediments at the opportunity landing site on Mars. Nature 438, 1123–1128. http://dx.doi.org/10.1038/nature04383.
Lamb, D., Verlinde, J., 2011. Physics and Chemistry of Clouds. Cambridge University Press, Cambridge, UK, pp. 205–213.
Langevin, Y. et al., 2005. Sulfates in the north polar region of Mars detected by OMEGA/Mars Express. Science 307, 1584–1586.
Lewis, K.W. et al., 2008. Quasi-periodic bedding in the sedimentary rock record of Mars. Science 322 (5907), 1532–1535. http://dx.doi.org/10.1126/science/1161870.
Louie, D.K., 2005. Handbook of Sulphuric Acid Manufacturing. DKL Engineering, Ontario Canada, pp. 17–38.
Malin, M.C., Edgett, K.S., 2000. Sedimentary rocks of early Mars. Science 290, 1927–1937. http://dx.doi.org/10.1126/science.290.5498.1927.
Malin, M.C., Edgett, K.S., 2003. Evidence for persistent flow and aqueous sedimentation on early Mars. Science 302, 1931. http://dx.doi.org/10.1126/science.1090544.
Manabe, S., Wetherald, R.T., 1967. Thermal equilibrium of the atmosphere with a given distribution of relative humidity. J. Atmos. Sci. 24, 241–259.
Mangold, N. et al., 2012. A chronology of early Mars climatic evolution from impact crater degradation. J. Geophys. Res. 117, E4. http://dx.doi.org/10.1029/2011JE004005.
Martin, S.T. et al., 1997. Phase transformations of micron-sized H_2SO_4/H_2O particles studied by infrared spectroscopy. J. Phys. Chem. 101, 5307–5313.
McCollum, T.M., Hynek, B.M., 2005. A volcanic environment for bedrock diagenesis at Meridiani Planum on Mars. Nature 438, 1129–1131.
McLennan, S.M. et al., 2014. Elemental geochemistry of sedimentary rocks at Yellowknife Bay, Gale Crater, Mars. Science 343, 6169. http://dx.doi.org/10.1126/science.1244734.
Meunier, A. et al., 2012. Magmatic precipitation as a possible origin of Noachian clays on Mars. Nat. Geosci. 5, 739–743. http://dx.doi.org/10.1039/NGEO1572.
Mills, M.J., 1996. Stratospheric Sulfate Aerosol: A Microphysical Model, Ph.D. Thesis. University of Colorado.
Mischna, M.A. et al., 2013. Effects of obliquity and water vapor/trace gas greenhouses in the early martian climate. J. Geophys. Res. 118, 560–576.
Moore, J.M. et al., 2003. Martian layered fluvial deposits: Implications for Noachian climate scenarios. Geophys. Res. Lett. 30 (24), 2292. http://dx.doi.org/10.1029/2003/GL019002.
National Institute for Occupational Safety and Health (NIOSH), 1981. Occupational Health Guidelines for Chemical Hazards, DHHS (NIOSH) Publication No. 81-123 <http://www.cdc.gov/niosh/81-123.html>.
Palmer, K.F., Williams, D., 1975. Appl. Opt. 14, 208–219.
Pham, M. et al., 1995. A three-dimensional study of the tropospheric sulfur cycle. J. Geophys. Res. 100, 26061–26092.
Phillips, R.J. et al., 2001. Ancient geodynamics and global-scale hydrology on Mars. Science 291, 2587–2591.
Pinto, J.P., Turco, R.P., Toon, O.B., 1989. Self-limiting physical and chemical effects in volcanic eruption clouds. J. Geophys. Res. 94 (D8), 11165–11174.
Pollack, J., 1979. Climatic change on the terrestrial planets. Icarus 37, 479–553.
Pollack, J. et al., 1987. The case for a wet, warm climate on early Mars. Icarus 71, 203–224.
Postawko, S.E., Kuhn, W.R., 1986. Effect of the greenhouse gases (CO_2, H_2O, SO_2) on martian paleoclimate. In: LPSC Proceedings, vol. 91, pp. D431–D438.
Poulet, F. et al., 2005. Phyllosilicates on Mars and implications for early martian climate. Nature 438, 623–627. http://dx.doi.org/10.1038/nature04274.
Ramirez, R.M. et al., 2014. Warming early Mars with CO_2 and H_2O. Nat. Geosci. 7, 59–63.
Righter, K., Pando, K., Danielson, L.R., 2009. Experimental evidence for sulfur-rich martian magmas: Implications for volcanism and surficial sulfur sources. Earth Planet. Space Lett. 288, 235–243.
Robbins, S.J., Di Achille, G., Hynek, B.M., 2011. The volcanic history of Mars: High-resolution crater-based studies of the calderas of 20 volcanoes. Icarus 211, 1179–1203.
Sagan, C., Toon, O.B., Gierasch, P.J., 1973. Climatic change on Mars. Science 181, 1045–1049. http://dx.doi.org/10.1126/science.181.4104.1045.
Sandor, B.J. et al., 2010. Sulfur chemistry in the Venus mesosphere from SO_2 and SO microwave spectra. Icarus 208, 49–60.
Sasson, R. et al., 1985. Optical properties of solid and liquid sulfur at visible and infrared wavelengths. Icarus 64, 368–374.
Schultz, P.H., 1985. The Martian Atmosphere Before and After the Argyre Impact. The MECA Workshop on the Evolution of the Martian Atmosphere, pp. 22–23.
Segura, T.L., Toon, O.B., Colaprete, A., 2008. Modeling the environmental effects of moderate-sized impacts on Mars. J. Geophys. Res. 113, E11007. http://dx.doi.org/10.1029/2008JE003147.
Settle, M., 1979. Formation and deposition of volcanic sulfate aerosols on Mars. J. Geophys. Res. 84, 8343–8354.
Sharp, R.P., Malin, M.C., 1975. Channels on Mars. Geol. Soc. Am. Bullet. 86, 593–609. http://dx.doi.org/10.1130/0016-7606(1975) 86.
Squyres, S.W., Kasting, J.F., 1994. Early Mars: How warm and how wet? Science 265, 744–749.
Squyres, S.W., Knoll, A.H., 2005. Sedimentary rocks at Meridiani Planum: Origin, diagenesis, and implications for life on Mars. Earth Planet. Sci. Lett. 240, 1–10.
Tian, F. et al., 2010. Photochemical and climate consequences of sulfur outgassing on early Mars. Earth Planet. Sci. Lett. 295, 412–418.
Tisdale, R.T. et al., 1998. Infrared optical constants of low-temperature H_2SO_4 solutions representative of stratospheric sulfate aerosols. J. Geophys. Res. Atm. 103 (D19), 25353–25370. http://dx.doi.org/10.1029/98JD02457.
Toon, O.B., Turco, R.P., Pollack, J.B., 1982. The ultraviolet absorber on Venus: Amorphous sulfur. Icarus 51, 358–373.
Toulmin III, P. et al., 1977. Geochemical and mineralogical interpretation of the Viking inorganic chemical results. J. Geophys. Res. 82, 4625–4634. http://dx.doi.org/10.1029/JS082i028p04625.
Urata, R.A., Toon, O.B., 2013. Simulations of the martian hydrologic cycle with a general circulation model: Implications for the ancient martian climate. Icarus 226, 229–250.
Wallace, D., Sagan, C., 1979. Evaporation of ice in planetary atmospheres: Ice-covered rivers on Mars. Icarus 39, 385–400.
Wordsworth, R., Forget, F., Eymet, V., 2010. Infrared collision-induced and far-line absorption in dense CO_2 atmospheres. Icarus 210, 992–997.
Wordsworth, R.D. et al., 2011. Gliese 581d is the first discovered terrestrial-mass exoplanet in the habitable zone. Astrophys. J. Lett. 733, L48. http://dx.doi.org/10.1088/2041-8205/733/2/L48.
Wordsworth, R. et al., 2013. Global modeling of the early martian climate under a denser CO_2 atmosphere: Water cycle and ice evolution. Icarus 222, 1–19.
Wordsworth, R., Kerber, L., Pierrehumbert, R.T., Forget, F., Head, J.W., 2015. Comparison of "warm and wet" and "cold and icy" scenarios for early Mars in a 3-D climate model. J. Geophys. Res. Planets 120, 1201–1219. http://dx.doi.org/10.1002/2015JE004787.
Yen, A.S. et al., 2005. An integrated view of the chemistry and mineralogy of martian soils. Nature 436, 49–54. http://dx.doi.org/10.1038/nature03637.
Young, A.T., 1977. An improved Venus cloud model. Icarus 32, 1–26. http://dx.doi.org/10.1016/0019-1035(77)90045-8.
Yung, Y.L., Nair, H., Gerstell, M.F., 1997. CO_2 greenhouse in the early martian atmosphere: SO_2 inhibits condensation. Icarus 130, 222–224.
Zent, A.P., Fanale, F.P., 1986. Possible Mars brines: Equilibrium and kinetic considerations. In: Proceedings of the 16th LPSC Conference, Part 2. J. Geophys. Res., 91(B4), pp. D439–D445.